Optimum Multiantenna Ambient Backscatter Receiver for Binary-Modulated Tag Signals

Hüseyin Yiğitler, Xiyu Wang, *Graduate Student Member, IEEE*, and Riku Jäntti, *Senior Member, IEEE*

***Abstract*— Ambient backscatter communication (AmBC) is becoming increasingly popular as a green Internet-of-things technology by enabling ultra-low-power data exchanges among simple tags. The bit-error-rate (BER) performance of the AmBC receivers is hampered by the low signal-to-interference-plus-noise ratio (SINR), which limits either the range or the data rate that can be supported by these systems. Among the alternatives, the solutions provided by a multiantenna receiver enable several practical methods to improve the SINR using array signal processing. In this paper, the optimum multiantenna AmBC receiver for any binary modulated tag signal is presented. Two receivers are derived from the maximum-a-posterior probability criterion for deterministic-unknown and for Gaussian distributed ambient signals. The closed-form cumulative distribution functions are derived for both of the receivers for performance evaluation purposes. It is discussed that these two receivers are equivalent under practical conditions, and the optimum receiver is a generalization of the multiantenna receivers available in the literature. Several implementation details are discussed, and numerical evaluation is provided to validate the development. Therefore, the presented receiver accommodates different tag modulations and achieves the best possible BER performance, which opens up new application possibilities by improving AmBC system flexibility.**

***Index Terms*— Ambient backscatter communication, Internet-of-Things, green communication, receiver design, receiver performance analysis.**

I. Introduction

INTERNET-OF-THINGS (IoT) technologies continue to be rolled out around the world to accommodate numerous use-cases with Internet connectivity. The total number of IoT devices is forecast to reach 25 billion in 2025 [1]. The increasing number of devices inevitably consumes a large amount of both energy and spectrum resources, which in turn limits the widespread deployments of IoT applications. The recently emerging ambient backscatter communication (AmBC) technology relieves both of these two limitations. In a foreseen AmBC deployment scenario (see Fig. 1a), a transmitter of an ambient system emits a radio frequency (RF) signal to serve its devices. A passive backscatter device (BD) of an AmBC system harvests energy from the pervasive ambient RF signal of the legacy transmitter to support its operations and to modulate its information. A composite signal traversing two paths, the *backscattered path* modulated by the BD, and the *direct path* that is not affected by BD operations, impinges at the AmBC receiver antenna. Then, the receiver uses the composite signal to decode the backscatter data. By requiring neither power-hungry nor expensive RF components for the transceiver circuits at the BD, the AmBC paradigm realizes the ultra-low-power and ultra-low-cost green communication [2]. It further provides significant bandwidth efficiency by enabling data exchange among the devices on the spectrum allocated for the ambient system. With these two inherent properties, AmBC is promising to become a crucial component for realizing sustainable IoT.

The main obstacle in front of widespread acceptance of the AmBC systems is the poor error-rate performance of its receiver. One factor that hampers the performance is the strong direct path interference (DPI), which is due to the tremendous power degradation experienced by the backscatter signal while propagating through the channels between transmitter and BD, and BD and receiver. The other factor is the lack of cooperation between the legacy and AmBC systems so that AmBC receivers have little information about the ambient signal. These two factors, in turn, degrades the signal-to-interference-plus-noise ratio (SINR) of the AmBC signal at the receiver, which is the main reason for poor receiver performance.

The SINR of the backscatter signal can be improved by exploiting frequency [3], [4], spatial [5], [6], [7], [8] or phase [9] differences between direct path signal and backscattered path signal, or using complex signal processing techniques to cancel the direct path signal [10]. Among these solutions, multiantenna receivers can mitigate the adverse impact of the DPI without the ambient system assistance or a need for information about the channels. A multiantenna receiver provides this option by solely exploiting the directional differences between the signals. Therefore, adopting multiple antennas at the receiver is a practically advantageous method for improving receiver performance.

Available works on multiantenna AmBC receivers mostly consider the BDs that perform on-off-keying (OOK) modulation. However, an OOK demodulator requires a higher SINR to achieve a certain bit-error-rate (BER)-performance

Manuscript received 3 November 2020; revised 1 April 2021, 22 October 2021, and 6 May 2022; accepted 7 August 2022. Date of publication 19 August 2022; date of current version 13 February 2023. This work was supported in part by the Academy of Finland through the *Backscatter Enabled Sustainable Monitoring Infrastructure for Assisted Living* (BESIMAL) Project under Project 33419. The associate editor coordinating the review of this article and approving it for publication was K. Huang. *(Corresponding author: Hüseyin Yiğitler.)*

The authors are with the Department of Communications and Networking, Aalto University, 02150 Espoo, Finland (e-mail: huseyin.yigitler@aalto.fi).

Color versions of one or more figures in this article are available at https://doi.org/10.1109/TWC.2022.3198514.

Digital Object Identifier 10.1109/TWC.2022.3198514

compared with the other binary demodulators. For instance, binary phase-shift keying (BPSK) demodulator can achieve the same BER performance with up to 6 dB less SINR. This gain, however, comes at the cost of solving several other practical problems and does not generalize well to all AmBC deployment conditions. For example, receiver symbol synchronization is more difficult for BPSK modulation than it is for OOK modulation. Therefore, having optimal receivers for different modulation techniques requires implementing different receivers, which restrains the system flexibility for adapting to different practical situations. In this regard, having a generalized optimal receiver that can support various binary-modulated signals is desirable, and the optimum multiantenna receiver for the binary-modulated backscatter signal for Gaussian distributed ambient signal has already been presented [8].

In this paper, an optimum multiantenna receiver, which works on any binary-modulated backscatter signal and all types of ambient signals, is presented. The receiver is derived from the maximum-a-posteriori probability (MAP) criterion, which yields a simple and clear structure. The resultant receiver avoids a complicated DPI cancellation and carrier and phase synchronization by exploiting the directional differences of the direct path and backscattered path signals impinging on the receiver antennas. Its performance primarily depends on the directional variation in the received signal. As such, if the direction of the composite signal changes with the backscatter symbol, its error rate decreases. Its operation has no constraint on the type of modulation of neither backscatter signal nor ambient signal, although its performance changes.

In this paper, we make the following contributions:

- We formulate and solve the optimum multiantenna receiver design problem for a general binary-modulated backscatter signal and for two types of ambient signal: i) deterministic-unknown ambient signal; and ii) Gaussian distributed ambient signal, which is equivalent to the optimal receiver presented in [8]. Both of the optimum receivers take a weighted square-sum form that can be implemented using two beamformers and a threshold device. Then, we show that these two receivers are equivalent under certain practical conditions. As such, this work generalizes the optimal receiver presented in [8] by discussing that Gaussian ambient signal assumption is not required for most of the practical scenarios.
- We derive the cumulative distribution functions of the test statistics for both of the optimum receivers. These functions are used for calculating the BER performance of the receivers. The resultant distributions have clear closed forms, and improves the derivations presented in [8]. The optimum receiver achieves the same BER-performance as the coherent receiver of the BPSK-modulated backscatter signal, although it avoids phase-coherent demodulation.
- We provide practical methods for estimating the beamformers that construct the test statistics of the optimal receivers. We discuss several practical implementation issues and provide solutions to the identified problems. In particular, we present an analog-digital hybrid implementation to solve dynamic range problem of AmBC receivers. We also compare the derived receiver with the available optimal receivers in the literature, specifically the receiver of [8].

The remainder of the paper is organized as follows. In Section II, the related works are reviewed, the notation used throughout the paper is introduced, and a general system model is given. The optimum receivers and their performance metric are derived in Section III. The implementation of the optimum receiver is discussed in Section IV. Simulation results are presented and discussed in Section V. Finally, conclusions are drawn in Section VI.

II. Background

In this section, we first summarize the related works. We give the general notations before introducing the system model and basic assumptions used throughout the paper.

A. Related Work

This paper aims to investigate the optimum multiantenna receiver for demodulating any binary-modulated backscatter signal. We first give a literature review for receivers of different binary modulated backscatter signal. Then, we review existing AmBC systems with a multiantenna receiver.

The low SINR at AmBC receiver has attracted a significant amount of interest in the literature, although available solutions for mitigating the impact of the strong DPI and unknown ambient signals mostly solve the problem for a specific setup. For backscatter devices adopting the OOK or differential BPSK modulations, the received signal strength varies as the BD switches the signal state according to its symbol. This property has motivated non-coherent receivers based on energy detector to average out the fast varying phases before comparing the energy levels associated with two backscatter signal states [2], [3], [6], [8], [10], [11], [12]. In these systems, DPI is mitigated by considering some specific properties of the legacy system. For orthogonal frequency division multiplexing (OFDM) ambient signal, the BD shifts the frequency of the ambient signal [4]. Since the coherent receiver requires lower SNR to achieve a BER value compared with that of a non-coherent receiver, it has also been investigated in the prior works. The receivers studied by Vougioukas *et al.* require phase estimate associated with BD operation and backscatter channel [13], and the one proposed by Yang *et al.* needs additional cooperation between the legacy system and backscatter system [10] because phases of both ambient signal and channels are not known to the receiver. Different from the receivers alluded above, in this work, we derive a more general receiver that has no constraint on the modulation type of the backscatter signal, special properties of the ambient signal and that does not require phase-coherent operation.

The attractive advantages of multiantenna AmBC receivers have recently motivated several works. The multiple antennas enable detecting a backscatter signal by using the variation in the signal strength [11], [14], or the phase [9] between antenna elements. However, these methods take advantage of the spatial diversity of the received signal among different

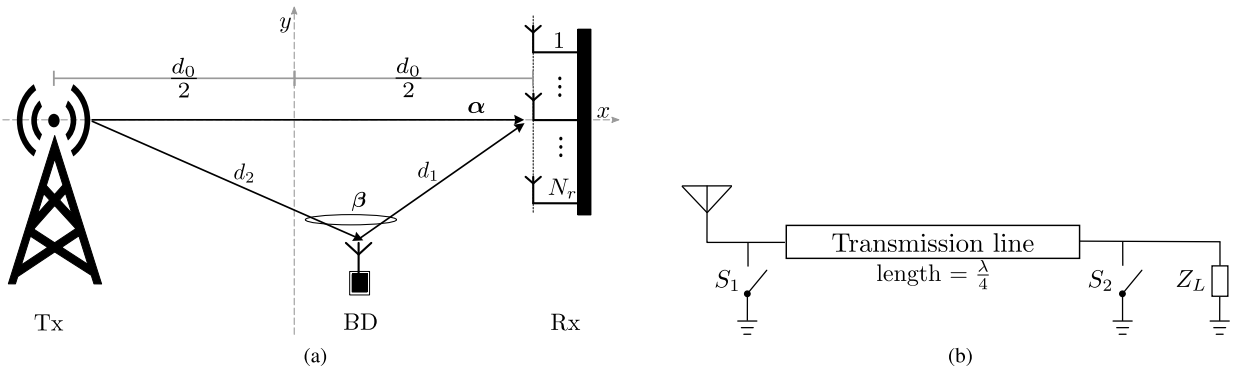

Fig. 1. In (a), an illustration of the AmBC systems. An ambient system transmitter (Tx) and the AmBC receiver (Rx) are placed on the horizontal axis of a Cartesian reference frame, the mid-point of the line segment connecting a reference Rx antenna to the Tx antenna is assigned as the reference frame origin. A backscatter device (BD) transmits its information by re-modulating the ambient system signal. The channel between Tx and Rx not affected by the BD operation is $\boldsymbol{\alpha}$, and the composite channel between the Tx and the BD, and the BD and the Rx is $\boldsymbol{\beta}$. In (b), a schematic design of a binary BD modulator using two switches and a quarter wavelength λ transmission line.

antennas but lose the array gain that can be provided by array signal processing. In contrast, our proposed receiver obtains array gain in addition to the diversity gain.

Recent works also exploit multiple antennas at the receiver to alleviate the adverse impact of both DPI and unknown ambient signals. Specifically, the multiantenna receiver enables mitigating the DPI by separating the desired backscatter signal from the direct path signal using beamforming without additional information about ambient signals or channels. The multiantenna receivers in [15] and [16] make use of an ensemble of temporal measurements in order to make a decision. Such receivers can only be implemented by oversampling when the BD is transmitting the same data bit. Such a design uses the time diversity [17, Sec. 3.2] as well as antenna diversity. In this paper, we take a holistic approach and derive the optimal receivers that can operate even when only a single temporal sample of a BD symbol is available.

The multiantenna receiver for BPSK modulated BD signals proposed by Duan *et al.* [7] aims at mitigating the impact of DPI while solving the dynamic-range problem of all-digital implementations. This receiver is heuristic in nature, and the authors neither studied optimality nor derived the receiver performance. The main idea of this receiver is improved by phase-coherent receivers recently investigated by our group [18], [19]. These receivers achieve a phase-coherent operation by using machine learning based phase estimators, which is then used by their demodulators. In this work, the derived optimum receiver is non-coherent, but it does not require marginalizing over the unknown phase of the BD symbol. Therefore, our receiver achieves the same performance as the coherent receivers although it does not require phase estimation.

The multiantenna receivers presented by Guo *et al.* [6] test the energy of the beamformed received signal to detect the OOK-modulated backscatter signal illuminated by Gaussian ambient signal. One of the receivers studied by the authors is the optimal multiantenna receiver for OOK modulated BD signal and Gaussian distributed ambient signal, which is a generalization of the single antenna optimal receiver presented in [20]. The same receiver has recently been studied by also Tao *et al.* [8], where the authors provide performance derivations in terms of BER. The optimal receiver of these works is the same as our optimal receiver for Gaussian distributed ambient signal. The main limitation of this receiver is due to Gaussian distributed ambient signal assumption, and cannot be generalized to all AmBC deployment conditions. The presented BER performance derivations in [8] have infinite series, which do not converge for all practical parameter ranges. In this work, we generalize the optimal receiver by separately considering deterministic-unknown ambient signals and Gaussian distributed ambient signals. We show that the optimal receiver for deterministic-unknown ambient signal can also be used for Gaussian signals without a significant performance loss for practical parameter ranges. Our BER performance derivations yield closed-form distributions. Furthermore, we thoroughly discuss the receiver and BD implementations, their practical implications on the receiver performance, and the conditions on preserving the optimality. Therefore, this work is holistic in nature so that the derived optimum receivers can be used in several AmBC systems, as such, it covers most of the reported receivers as its special cases.

B. Notations

Throughout the paper, scalars are denoted by italic font letters a, vectors and matrices are represented by lower-case $\boldsymbol{a}$ and upper-case $\boldsymbol{A}$ boldface italic letters, respectively. Complex scalars are assumed, and their set is denoted by $\mathbb{C}$. The Euclidean norm of a vector $\boldsymbol{a}$ is represented by $\|\boldsymbol{a}\|$ and the absolute value of a is represented by $|a|$. The $n \times n$ identity matrix is $\boldsymbol{I}_n$, and the subscript n may be omitted sometimes for simplicity. The conjugate-transpose, conjugate, and transpose of a matrix $\boldsymbol{A}$ are $\boldsymbol{A}^H$, $\boldsymbol{A}^*$ and $\boldsymbol{A}^T$, respectively. The trace, the rank and the determinant of a matrix $\boldsymbol{A}$ are represented by $\mathrm{Tr}(\boldsymbol{A})$, $\mathrm{rank}(\boldsymbol{A})$ and $|\boldsymbol{A}|$. The distribution of a complex Gaussian random vector is $\mathcal{N}(\boldsymbol{a}, \boldsymbol{A})$, and $\mathcal{CN}(\boldsymbol{a}, \boldsymbol{A})$ denotes circularly symmetric complex Gaussian vector [21, sec. 7.8] with mean $\boldsymbol{a}$ and covariance matrix $\boldsymbol{A}$. The statistical expectation is $\mathbb{E}\{\cdot\}$. The imaginary unit is $j = \sqrt{-1}$.

C. System Model

In this paper, a typical bi-static narrow-band AmBC system, depicted in Fig. 1a, is considered. An ambient system serves its devices with the ambient signal source (Tx), while an AmBC receiver (Rx) with N_r-antenna linear array is decoding the backscatter signal emitted by a single-antenna backscatter device (BD). Three nodes are placed in the Cartesian reference frame of a two-dimensional Euclidean space, as shown in Fig. 1a. The $\lceil N_r/2 \rceil$-th antenna of the Rx is selected as the reference antenna, where $\lceil \cdot \rceil$ denotes the ceiling function, which assumes the least integer greater than or equal to its argument. The line segment connecting the Tx antenna and the Rx reference antenna is set as the x-axis of the reference frame, and its midpoint is selected as the origin. In this reference frame, the locations of the Tx, the BD and the i-th Rx antenna (for $i = 1, \cdots, N_r$) are denoted by $\boldsymbol{p}_t$, $\boldsymbol{p}$ and $\boldsymbol{p}_{r,i}$, respectively. Then, the distances between the Tx and the i-th Rx antenna, the BD and the i-th Rx antenna, and the Tx and the BD are

$$d_{0,i} = \|\boldsymbol{p}_t - \boldsymbol{p}_{r,i}\|, \quad d_{1,i} = \|\boldsymbol{p} - \boldsymbol{p}_{r,i}\|, \quad \text{and} \quad d_2 = \|\boldsymbol{p}_t - \boldsymbol{p}\|,$$

respectively. For notational simplicity, the distances between the Tx and the Rx reference antenna, and the BD and the reference Rx antenna are denoted by d_0 and d_1, respectively. The distance between the Tx and the Rx also refers to d_0, and the distance between the BD and the Rx refers to d_1.

In the following, we assume a narrow-band receiver, which cannot resolve individual multipath components. For this system, the vector $\boldsymbol{\alpha} = [\alpha_1, \cdots, \alpha_{N_r}]^T$ denotes the channel gains of the direct path observed by each Rx antenna. The components of $\boldsymbol{\alpha}$ are the phasor sum of all multi-path components that are not affected by the operation of the BD. Let us denote the vector composed of the phasor sum of all other multi-path components, which are affected by the operation of the BD, by $\boldsymbol{\beta} = [\beta_1, \cdots, \beta_{N_r}]^T$. We refer to $\boldsymbol{\alpha}$ as the *direct path channels*, and $\boldsymbol{\beta}$ as the *backscatter path channels*. For a quasi-static deployment, the coherence time of the channels exceeds the duration of several BD symbols, that is, the received signal experiences a block-fading, so that the channels stay constant for a duration.[1] Although the channels $\boldsymbol{\alpha}$ and $\boldsymbol{\beta}$ experience independent fading realizations, their large-scale spatial average can be calculated using the deployment geometry and free-space path-loss model as

$$\begin{aligned} \alpha_i &= \rho_\alpha \frac{c_0/f_c}{4\pi d_{0,i}} \exp\left(j2\pi \frac{d_{0,i}}{c_0/f_c}\right), \\ \beta_i &= \rho_\beta \frac{c_0/f_c}{4\pi d_2} \frac{c_0/f_c}{4\pi d_{1,i}} \exp\left(j2\pi \frac{d_{1,i}+d_2}{c_0/f_c}\right), \end{aligned} \tag{1}$$

where f_c is the carrier frequency and c_0 is the free-space electromagnetic propagation speed, c_0/f_c is the wavelength; ρ_α and ρ_β are fading losses in the current fading block affecting the direct path channels and backscattering path channels in respective order.

[1]For a deployment experiencing block-fading, it is customary to assume that the channels stay approximately constant for a duration longer than the longest BD frame, which is often referred to as a codeword block, so that the channels' estimates stay valid within a BD frame. However, both of the channels may assume different realizations among different blocks.

Let us denote the binary-modulated backscatter signal transmitted by the BD as x, and the unknown ambient signal transmitted by the Tx as $\bar{s}$. The k-th digital sample of the receiver can be written as

$$\boldsymbol{y}[k] = \boldsymbol{\alpha}\bar{s}[k] + \boldsymbol{\beta}\bar{s}[k]x[k] + \boldsymbol{n}[k],$$

where $x[k]$ is the BD symbol and $\bar{s}[k]$ is the ambient signal during the k-th sample, and $\boldsymbol{n}$ is standard circularly-symmetric complex Gaussian noise, whose components are independent of x and $\bar{s}$. The received signal-to-noise ratio (SNR) of the direct path signal at the i-th antenna is $|\alpha_i|^2|\bar{s}|^2$, since the components of the noise $\boldsymbol{n}$ have unity variance.[2] It follows that the average SNR[3] is

$$\gamma \triangleq \|\boldsymbol{\alpha}\bar{s}\|^2/N_r. \tag{2}$$

The amplitude of the ambient signal can be represented by the observed average SNR γ and $\|\boldsymbol{\alpha}\|^2$. Then, the ambient signal can be defined as

$$s \triangleq \frac{\sqrt{\gamma N_r}}{\|\boldsymbol{\alpha}\|} \frac{\bar{s}}{|\bar{s}|}. \tag{3}$$

The ratio of average channel gains of the direct and the backscattered path signals is $\|\boldsymbol{\alpha}\|^2/\|\boldsymbol{\beta}\|^2$. It is discussed in [18] thoroughly that this ratio can reach up to 40 dB when the BD is 5 meters away from the Rx. Therefore, the backscattered path signal has a particularly low SNR, which should be improved by the receiver to reach an acceptable error-rate performance.

In this paper, the BD adopts a binary modulation $x \in \mathcal{X} = \{x_0, x_1\}$ using the BD design shown in Fig. 1. This design is a realization of well-studied backscatter modulators, e.g., in [22], which are also used for ambient BD design in [23]. It can be used for implementing BPSK modulation by closing one of the switches S_1 and S_2 depending on the BD symbol, e.g., when $x = x_0$, S_1 is closed while keeping S_2 open; when $x = x_1$, S_2 is closed while S_1 is open. It can also realize OOK modulation by keeping either S_1 or S_2 open and opening/closing the other switch. The impact of the BD implementation on the receiver performance is discussed in Sec. IV-B2.

For the considered AmBC system, the duration of x is longer than the duration of the ambient symbol s so that each temporal sample of the received signal $\boldsymbol{y}[k]$ is affected by independent symbol of s. Now, let us denote the compound channel by $\boldsymbol{g}_\ell$ so that the received signal reads as

$$\boldsymbol{g}_\ell \triangleq \boldsymbol{g}(x_\ell) = \boldsymbol{\alpha} + \boldsymbol{\beta}x_\ell, \quad \boldsymbol{y}[k] = \boldsymbol{g}(x_\ell)s[k] + \boldsymbol{n}[k], \tag{4}$$

for $\ell = 0, 1$. In the following, we occasionally drop the time dependence of $\boldsymbol{y}$ when the content is restricted to a single temporal measurement sample.

[2]The variance of the noise process is mainly defined by the receiver hardware quality including the quantization noise variance. By assuming unity variance noise, we implicitly assign a higher transmit power, and use the SNR as a replacement of signal power. For a receiver with an acceptable sensitivity level, 30 dB SNR does not require the receiver to be very close to the transmitter in terms of wavelengths.

[3]The total received SNR for N_r-antenna receiver is $\|\boldsymbol{\alpha}\bar{s}\|^2$, where $N_r|\bar{s}|^2$ is the *array gain*, and $\|\boldsymbol{\alpha}\|^2/N_r$ is the *diversity gain* [17, Sec. 3.3.1]. In this paper, we follow this definition of the total received SNR, and ignore the divergence of array gain when $N_r \to \infty$.

III. Optimum multiantenna Receiver

In this section, the optimum multiantenna receiver for binary-modulated backscatter signal is derived for two cases: deterministic-unknown ambient signal and Gaussian distributed ambient signal together with their performances analyses. The practical implementations details of the optimum receiver are discussed in the next section.

The optimum receiver of a binary-modulated signal makes a decision using the MAP principle, which chooses the symbol that has a higher posterior probability for a given measurement [24, ch. 4], that is

$$\Pr\{x = x_0|\boldsymbol{y}\} \underset{\mathcal{H}_1}{\overset{\mathcal{H}_0}{\gtrless}} \Pr\{x = x_1|\boldsymbol{y}\}, \tag{5}$$

where the null hypothesis $\mathcal{H}_0$ is x_0 *is transmitted*, and $\mathcal{H}_1$ is the alternative hypothesis. For a random vector $\boldsymbol{y}$ with probability density function (PDF) $f(\boldsymbol{y})$, the posterior probabilities can be computed using Bayes' Theorem

$$\Pr\{x = x_\ell|\boldsymbol{y}\} = \frac{f(\boldsymbol{y}|x = x_\ell)\Pr\{x = x_\ell\}}{f(\boldsymbol{y})}, \quad \text{for } \ell = 0, 1.$$

Since the denominator is common under two hypothesis and the BD adopts binary modulation, MAP criterion can be written as

$$f(\boldsymbol{y}|x = x_0)q \underset{\mathcal{H}_1}{\overset{\mathcal{H}_0}{\gtrless}} f(\boldsymbol{y}|x = x_1)(1 - q), \tag{6}$$

where we have defined $\Pr\{x = x_0\} = q$, which leaves $\Pr\{x = x_1\} = 1 - q$.

The likelihood functions and prior BD symbol probabilities yield a test statistic z and a threshold value V to make a decision. Once the distribution of z is determined, performance of a receiver is quantified by its probability of error, which is the average of the *probability of false alarm* (also known as Type-I error) P_f and the *probability of miss* (also known as Type-II error) P_m. For the problem at hand, these probabilities are given by

$$\begin{aligned} &P_f = (1 - F_z(V|x = x_0)), \quad P_m = F_z(V|x = x_1), \\ &P_e = qP_f + (1 - q)P_m, \end{aligned} \tag{7}$$

where $F_z(\cdot|x)$ is the conditional cumulative distribution function (CDF) of the test statistic z.

For the AmBC receivers that are implemented independent of the ambient receiver, the ambient signal s is not available. For this case, the receiver design problem should be solved by assuming certain signal type for s, which changes the likelihood functions in Eq. (6). In the sequel, we consider two types of s. The worst case is when the AmBC receiver has no prior knowledge about the ambient signal so that s is treated as a deterministic-unknown parameter. Since we restrict the scope to the receivers that can sample at the rate or slower than the data rate of the ambient signal, the ambient signal s affecting the measurement $\boldsymbol{y}$ is also an unknown constant. The other case is when the receiver assumes a prior distribution for s. In particular, it can be assumed as a zero-mean Gaussian with constant variance. This prior arises in many practical ambient signal sources with fast amplitude variation. Therefore, these two cases arise frequently in practice, and each can be useful for an AmBC deployment.

A. Deterministic and Unknown Ambient Signal

We first consider the ambient signal s as a constant that can be estimated using a single temporal measurement $\boldsymbol{y}$ so that s is an unknown parameter that defines the distribution of $\boldsymbol{y}$. In this subsection, we first derive the optimal receiver, and then elaborate on its performance.

1) Receiver Design: In case s is an unknown constant, the likelihood functions in Eq. (6) can be obtained by first estimating s as $\hat{s}$. Now, the measurement has a joint distribution of the estimation error $\varepsilon_s = s - \hat{s}$ and the measurement noise $\boldsymbol{n}$. Then, the likelihood functions are obtained by marginalizing ε_s out,

$$f(\boldsymbol{y}|x = x_\ell) = \int_{\mathbb{S}} f(\boldsymbol{y}|x = x_\ell, \varepsilon_s) f(\varepsilon_s) d\varepsilon_s, \tag{8}$$

where $\mathbb{S}$ is the support of the ambient signal estimation error ε_s, and $f(\varepsilon_s)$ denotes its PDF. Thus, the marginal density of ε_s and the conditional density $f(\boldsymbol{y}|x = x_\ell, \varepsilon_s)$ are required to find the likelihoods.

Let us suppose that the N_r measurements of a multiantenna receiver $\boldsymbol{y}$ is used by an unbiased and efficient estimator to obtain an estimate of the ambient signal as $\hat{s}$. These requirements are readily satisfied by Maximum Likelihood estimator [25, ch. 5], and its estimate $\hat{s}$ using the measurement vector $\boldsymbol{y}$ for a given $x = x_\ell$ value, and associated estimation error ε_s are

$$\hat{s} = \frac{\boldsymbol{g}_\ell^H \boldsymbol{y}}{\|\boldsymbol{g}_\ell\|^2}, \qquad \varepsilon_s = \hat{s} - s = \frac{\boldsymbol{g}_\ell^H \boldsymbol{n}}{\|\boldsymbol{g}_\ell\|^2}.$$

The estimation error ε_s is complex Gaussian random variable with

$$\mathbb{E}\{\varepsilon_s\} = 0, \quad \mathbb{E}\{\varepsilon_s \varepsilon_s^*\} = 1/\|\boldsymbol{g}_\ell\|^2.$$

As the number of receiver antennas N_r increases, $\|\boldsymbol{g}_\ell\|^2$ monotonically increases, and $\mathbb{E}\{\varepsilon_s \varepsilon_s^*\} \to 0$. This, in turn, implies that $f(\varepsilon_s) \to \delta(\varepsilon_s)$ in mean square, where $\delta(\cdot)$ is the Dirac delta function, so that this estimator is asymptotically consistent.

The density function of the estimation error ε_s and the conditional distribution of the measurement is required to marginalize ε_s. For this purpose, substituting $\hat{s}$ into Eq. (4) yields

$$\boldsymbol{y} = \hat{s}\boldsymbol{g}_\ell + \tilde{\boldsymbol{n}}, \quad \tilde{\boldsymbol{n}} \triangleq \boldsymbol{n} - \varepsilon_s \boldsymbol{g}_\ell = \left(\boldsymbol{I} - \frac{\boldsymbol{g}_\ell \boldsymbol{g}_\ell^H}{\|\boldsymbol{g}_\ell\|^2}\right)\boldsymbol{n}. \tag{9}$$

Hence, the conditional distribution of the measurement $\boldsymbol{y}$, when $x = x_\ell$ and ε_s are given, is $\mathcal{N}(\boldsymbol{\mu}_{\boldsymbol{y}|x_\ell,\varepsilon_s}, \boldsymbol{\Sigma}_{\boldsymbol{y}|x_\ell,\varepsilon_s})$ with

$$\begin{aligned} &\boldsymbol{\mu}_{\boldsymbol{y}|x_\ell,\varepsilon_s} = \hat{s}\boldsymbol{g}_\ell, \quad \boldsymbol{\Sigma}_{\boldsymbol{y}|x_\ell,\varepsilon_s} = \boldsymbol{G}_d(x_\ell), \\ &\boldsymbol{G}_d(x_\ell) \triangleq \boldsymbol{I} - \frac{\boldsymbol{g}_\ell \boldsymbol{g}_\ell^H}{\|\boldsymbol{g}_\ell\|^2}. \end{aligned} \tag{10}$$

It follows that Eq. (6) is obtained by substituting the PDF of $\mathcal{N}(\boldsymbol{\mu}_{\boldsymbol{y}|x_\ell,\varepsilon_s}, \boldsymbol{\Sigma}_{\boldsymbol{y}|x_\ell,\varepsilon_s})$ as a likelihood function, since the integral in Eq. (8) results the conditional PDF. Then, taking

the logarithm of both sides yields the binary hypothesis test for the optimal receiver as

$$\ln f(\boldsymbol{y}|x=x_0,\varepsilon_s) \underset{\mathcal{H}_1}{\overset{\mathcal{H}_0}{\gtrless}} \ln f(\boldsymbol{y}|x=x_1,\varepsilon_s) + \ln\left(\frac{1-q}{q}\right). \tag{11}$$

The conditional density of the measurement $\boldsymbol{y}$, when $x=x_\ell$ and ε_s are given, is a degenerate multi-variate Gaussian, of which, PDF does not exist in $\mathbb{C}^{N_r}$, but it can be defined in a subspace [26, Sec. 8a.4]. Since the conditional covariance matrix $\boldsymbol{G}_d(x_\ell)$ is idempotent matrix of rank N_r-1, the conditional PDF can be defined in the (N_r-1)-dimensional subspace as

$$f(\boldsymbol{y}|x=x_\ell,\varepsilon_s) = \frac{\exp\left(-\left(\boldsymbol{y}-\boldsymbol{g}_\ell\hat{s}\right)^H \boldsymbol{G}_d(x)^\dagger \left(\boldsymbol{y}-\boldsymbol{g}_\ell\hat{s}\right)\right)}{\pi^{N_r-1}\det{}^*(\boldsymbol{G}_d(x))},$$

where $\det{}^*(\boldsymbol{G}_d(x))$ is the product of non-zero eigenvalues of $\boldsymbol{G}_d(x)$, which is equal to 1, and $\boldsymbol{G}_d(x)^\dagger$ denotes Moore–Penrose generalized inverse of $\boldsymbol{G}_d(x)$, which, in our case, is $\boldsymbol{G}_d(x)$ itself.

If the receiver can oversample with respect to the BD symbol data rate, but the sampling rate is slower than the data rate of ambient signal s, it might acquire K samples for one BD symbol, which we refer to as *oversampling rate*. Since the noise samples $\boldsymbol{n}[k]$ are independent in time, it follows that the received signal samples conditioned on x_ℓ and $\varepsilon_s[k]$ are independent, and their joint density is just their respective products. Then, taking the logarithm of the conditional joint PDF yields

$$\begin{aligned}\ln f(\boldsymbol{y}[1],\cdots,\boldsymbol{y}[K]|x=x_\ell,s=\hat{s})& \\ = -(N_r-1)K\ln\pi - \sum_{k=1}^{K}\boldsymbol{y}^H[k]\boldsymbol{G}_d(x_\ell)\boldsymbol{y}[k].&\end{aligned} \tag{12}$$

Now, substituting log-likelihood functions for two possible values of x into Eq. (11) for K samples, the binary hypotheses test simplifies to

$$\sum_{k=1}^{K}\boldsymbol{y}^H[k]\big(\boldsymbol{G}_d(x_1)-\boldsymbol{G}_d(x_0)\big)\boldsymbol{y}[k] \underset{\mathcal{H}_1}{\overset{\mathcal{H}_0}{\gtrless}} K\ln\left(\frac{1-q}{q}\right). \tag{13}$$

Therefore, the optimum receiver first needs to calculate the test statistic z_d,

$$z_d \triangleq \sum_{k=1}^{K}\boldsymbol{y}^H[k]\left(\frac{\boldsymbol{g}_0\boldsymbol{g}_0^H}{\|\boldsymbol{g}_0\|^2}-\frac{\boldsymbol{g}_1\boldsymbol{g}_1^H}{\|\boldsymbol{g}_1\|^2}\right)\boldsymbol{y}[k], \tag{14}$$

and then compares its output value with the decision threshold $V_d=0$ when BD symbols have equal probability.

2) Receiver Performance: In order to investigate the distribution of the test statistic z_d in Eq. (14), let us first define the matrix

$$\boldsymbol{M}_d = \frac{\boldsymbol{g}_0\boldsymbol{g}_0^H}{\|\boldsymbol{g}_0\|^2}-\frac{\boldsymbol{g}_1\boldsymbol{g}_1^H}{\|\boldsymbol{g}_1\|^2}, \tag{15}$$

so that $z_d=\boldsymbol{y}^H\boldsymbol{M}_d\boldsymbol{y}$. Since the distribution of the quadratic form defining z_d is a function of spectral properties of $\boldsymbol{M}_d$, the following proposition provides the key ingredient in deriving the conditional density functions of z_d under two hypothesis.

Proposition 1: The matrix $\boldsymbol{M}_d$ is a rank-2 indefinite Hermitian matrix with the non-zero eigenvalues

$$\lambda_1(\boldsymbol{M}_d) = -\lambda_2(\boldsymbol{M}_d) = \kappa = \sqrt{1-\frac{|\boldsymbol{g}_0^H\boldsymbol{g}_1|^2}{\|\boldsymbol{g}_0\|^2\|\boldsymbol{g}_1\|^2}}, \tag{16}$$

and the corresponding normalized eigenvectors

$$\boldsymbol{u}_1 = \sqrt{\frac{1-\kappa}{2\kappa^2}}\left(\boldsymbol{I}+\frac{1}{\kappa-1}\frac{\boldsymbol{g}_0\boldsymbol{g}_0^H}{\|\boldsymbol{g}_0\|^2}\right)\frac{\boldsymbol{g}_1}{\|\boldsymbol{g}_1\|}, \tag{17a}$$

$$\boldsymbol{u}_2 = \sqrt{\frac{1+\kappa}{2\kappa^2}}\left(\boldsymbol{I}-\frac{1}{\kappa+1}\frac{\boldsymbol{g}_0\boldsymbol{g}_0^H}{\|\boldsymbol{g}_0\|^2}\right)\frac{\boldsymbol{g}_1}{\|\boldsymbol{g}_1\|}, \tag{17b}$$

when $\kappa\neq 1$, and when $\kappa=1$, eigenvectors are $\boldsymbol{u}_1=\boldsymbol{g}_1/\|\boldsymbol{g}_1\|$ and $\boldsymbol{u}_2=\boldsymbol{g}_0/\|\boldsymbol{g}_0\|$.

Proof: See Appendix A. ∎

Since $\boldsymbol{M}_d$ is a rank-2 matrix, its spectral decomposition is given by $\boldsymbol{M}_d=\kappa(\boldsymbol{u}_1\boldsymbol{u}_1^H-\boldsymbol{u}_2\boldsymbol{u}_2^H)$, so that the test statistic z_d can be written as

$$z_d = \kappa\left(\underbrace{\sum_{k=1}^{K}|\boldsymbol{u}_1^H\boldsymbol{y}[k]|^2}_{t}-\underbrace{\sum_{k=1}^{K}|\boldsymbol{u}_2^H\boldsymbol{y}[k]|^2}_{r}\right)\underset{\mathcal{H}_1}{\overset{\mathcal{H}_0}{\gtrless}}0. \tag{18}$$

The random variables t and r are independent and non-central chi-square distributed [27, ch. 2], both with degrees of freedom $2K$ and variance $1/2$, but with different non-centrality parameters given by

$$\begin{aligned}\theta_t(x_\ell) &= 2|\boldsymbol{u}_1^H\boldsymbol{g}_\ell|^2\sum_{k=1}^{K}|s[k]|^2 \\ &= \|\boldsymbol{g}_\ell\|^2(1+(-1)^\ell\kappa)\sum_{k=1}^{K}|s[k]|^2,\end{aligned} \tag{19a}$$

$$\begin{aligned}\theta_r(x_\ell) &= 2|\boldsymbol{u}_2^H\boldsymbol{g}_\ell|^2\sum_{k=1}^{K}|s[k]|^2 \\ &= \|\boldsymbol{g}_\ell\|^2(1-(-1)^\ell\kappa)\sum_{k=1}^{K}|s[k]|^2.\end{aligned} \tag{19b}$$

The distribution of the test statistic in Eq. (18) can be obtained by defining it as a difference of two independent non-central chi-square variables t and r, of which density is given in [28]. However, the resultant density function does not converge for the parameter ranges we are interested in. An alternative approach is to define the ratio of t and r as the test statistic,

$$z_r \triangleq \frac{t}{r}\underset{\mathcal{H}_1}{\overset{\mathcal{H}_0}{\gtrless}}1.$$

so that it is compared against threshold value $V_r=1$. The test statistic z_r is a doubly non-central F random variable [29,

ch. 30], of which CDF reads as

$$F(z_r|x=x_\ell) = \exp\left(\frac{\|s\boldsymbol{g}_\ell\|^2}{2}\right) \times \sum_{i=0}^{\infty}\sum_{j=0}^{\infty} \frac{\theta_r^i(x_\ell)\theta_t^j(x_\ell)}{i!j!}\frac{1}{2^{i+j}}\bar{B}_{\frac{z_r}{z_r+1}}(i+K, j+K), \tag{20}$$

where $\bar{B}_x(a,b)$ denotes the (regularized) incomplete Beta function [30, Sec. 26.5]. The main difficulty in calculating the probability of error in Eq. (7) using Eq. (20) is slow convergence of the sums as discussed thoroughly by Paolella [31, Sec. 10.2]. This problem is usually overcome by utilizing an approximation of the exact CDF. In the following sections, probability of error is calculated using the saddle point approximation.

B. Gaussian Distributed Ambient Signal

When the distribution of s is given, the individual components of $\boldsymbol{y}$ has a joint distribution of s, x and $\boldsymbol{n}$. Then, the likelihood $f(\boldsymbol{y}|x=x_\ell)$ can be derived using the independence of these random variables. In this subsection, we assume that the ambient signal is $s \sim \mathcal{N}(0,\sigma_s^2)$, and we first derive the optimal receiver, and then study its error performance.

1) Receiver Design: For a Gaussian distributed s, the measurement $\boldsymbol{y}$ has the Gaussian density function, but it is not a multivariate Gaussian distributed random variable. However, the conditional densities for a given BD symbol $x = x_\ell$ are jointly Gaussian with mean $\boldsymbol{0}$ and conditional covariance matrix $\boldsymbol{\Sigma}_{\boldsymbol{y}|x_\ell}$. It is straightforward to show that

$$\boldsymbol{\Sigma}_{\boldsymbol{y}|x_\ell} = \sigma_s^2\boldsymbol{g}_\ell\boldsymbol{g}_\ell^H + \boldsymbol{I}. \tag{21}$$

The conditional covariance matrix has a full rank, and its eigenvalues are $\{1+\sigma_s^2\|\boldsymbol{g}_\ell\|^2, 1, \cdots, 1\}$. Thus, the conditional PDF exists, and it is given by

$$f(\boldsymbol{y}|x=x_\ell) = \frac{1}{\pi^{N_r}|\boldsymbol{\Sigma}_{\boldsymbol{y}|x_\ell}|}\exp\left(-\boldsymbol{y}^H\boldsymbol{\Sigma}_{\boldsymbol{y}|x_\ell}^{-1}\boldsymbol{y}\right). \tag{22}$$

It follows from the definition of the conditional covariance matrix that

$$\boldsymbol{\Sigma}_{\boldsymbol{y}|x_\ell}^{-1} = \boldsymbol{I} - \frac{\sigma_s^2\boldsymbol{g}_\ell\boldsymbol{g}_\ell^H}{1+\sigma_s^2\|\boldsymbol{g}_\ell\|^2}, \quad |\boldsymbol{\Sigma}_{\boldsymbol{y}|x_\ell}| = 1+\sigma_s^2\|\boldsymbol{g}_\ell\|^2.$$

Let us make the following definitions to simplify the notations,

$$c_\ell \triangleq \frac{\sigma_s^2\|\boldsymbol{g}_\ell\|^2}{1+\sigma_s^2\|\boldsymbol{g}_\ell\|^2}, \quad \boldsymbol{G}_g(x_\ell) \triangleq \boldsymbol{I} - c_\ell\frac{\boldsymbol{g}_\ell\boldsymbol{g}_\ell^H}{\|\boldsymbol{g}_\ell\|^2}. \tag{23}$$

In case the receiver can acquire K samples in a BD symbol duration, the joint conditions density of $\boldsymbol{y}[k]$ for $k=1,\cdots,K$ is the product of individual samples due to the independence of noise process samples. Then, after substituting K products of Eq. (22) into Eq. (6), and taking the logarithm of both sides, the binary hypotheses test for a general binary-modulated backscatter signal and a Gaussian distributed ambient signal is obtained as

$$\sum_{k=1}^{K}\boldsymbol{y}[k]^H\left(\boldsymbol{G}_g(x_1)-\boldsymbol{G}_g(x_0)\right)\boldsymbol{y}[k] \underset{\mathcal{H}_1}{\overset{\mathcal{H}_0}{\gtrless}} K\ln\left(\frac{1-q}{q}\frac{1+\sigma_s^2\|\boldsymbol{g}_0\|^2}{1+\sigma_s^2\|\boldsymbol{g}_1\|^2}\right). \tag{24}$$

The test statistic z_g and the decision threshold V_g for equally probable BD symbols for this case are

$$z_g \triangleq \frac{1}{K}\sum_{k=1}^{K}\boldsymbol{y}^H[k]\left(c_0\frac{\boldsymbol{g}_0\boldsymbol{g}_0^H}{\|\boldsymbol{g}_0\|^2} - c_1\frac{\boldsymbol{g}_1\boldsymbol{g}_1^H}{\|\boldsymbol{g}_1\|^2}\right)\boldsymbol{y}[k],$$
$$V_g \triangleq \ln\left(\frac{1+\sigma_s^2\|\boldsymbol{g}_0\|^2}{1+\sigma_s^2\|\boldsymbol{g}_1\|^2}\right). \tag{25}$$

Therefore, the optimal receiver for this case, first calculates the test statistic z_g, and then compares its value with V_g.

2) Receiver Performance: The test statistic z_g is a quadratic form, and it is a Gaussian quadratic form for a given BD symbol x. In order to obtain its distribution under two hypothesis, let us first define,

$$\boldsymbol{M}_g \triangleq c_0\frac{\boldsymbol{g}_0\boldsymbol{g}_0^H}{\|\boldsymbol{g}_0\|^2} - c_1\frac{\boldsymbol{g}_1\boldsymbol{g}_1^H}{\|\boldsymbol{g}_1\|^2}. \tag{26}$$

Then, z_g can be written as

$$z_g = \sum_{k=1}^{K}\boldsymbol{v}^H[k]\frac{1}{K}\boldsymbol{\Sigma}_{\boldsymbol{y}|x_\ell}^{1/2}\boldsymbol{M}_g\boldsymbol{\Sigma}_{\boldsymbol{y}|x_\ell}^{1/2}\boldsymbol{v}[k], \tag{27}$$

where $\boldsymbol{v}[k]$ are independent and standard Gaussian $\boldsymbol{v}[k] \sim \mathcal{N}(\boldsymbol{0},\boldsymbol{I})$. Since the distribution of this quadratic form depends on the eigenvalues of the matrix $\boldsymbol{\Sigma}_{\boldsymbol{y}|x_\ell}^{1/2}\boldsymbol{M}_g\boldsymbol{\Sigma}_{\boldsymbol{y}|x_\ell}^{1/2}/K$, the following proposition is crucial.

Proposition 2: The matrix $\boldsymbol{W}_\ell = \boldsymbol{\Sigma}_{\boldsymbol{y}|x_\ell}^{1/2}\boldsymbol{M}_g\boldsymbol{\Sigma}_{\boldsymbol{y}|x_\ell}^{1/2}/K$ is a rank-2 indefinite Hermitian matrix with non-zero eigenvalues

$$\lambda_{1,2}(\boldsymbol{W}_0) = \frac{1}{2K}\left(c_1-\sigma_s^2\|\boldsymbol{g}_0\|^2\kappa_1^2\right) \pm\frac{1}{2K}\sqrt{(c_1+\sigma_s^2\|\boldsymbol{g}_0\|^2\kappa_1^2)^2 - 4\,c_1\frac{\|\boldsymbol{g}_0\|^2}{\|\boldsymbol{g}_1\|^2}(1-\kappa_1^2)} \tag{28a}$$

$$\lambda_{1,2}(\boldsymbol{W}_1) = \frac{1}{2K}\left(-c_0+\sigma_s^2\|\boldsymbol{g}_1\|^2\kappa_0^2\right) \pm\frac{1}{2K}\sqrt{(c_0+\sigma_s^2\|\boldsymbol{g}_1\|^2\kappa_0^2)^2 - 4\,c_0\frac{\|\boldsymbol{g}_1\|^2}{\|\boldsymbol{g}_0\|^2}(1-\kappa_0^2)} \tag{28b}$$

where we have defined

$$\kappa_\ell = \sqrt{1-c_l\frac{|\boldsymbol{g}_0^H\boldsymbol{g}_1|^2}{\|\boldsymbol{g}_0\|^2\|\boldsymbol{g}_1\|^2}} \qquad \text{for } \ell=0,1. \tag{29}$$

Proof: See Appendix B. ∎

The distribution of the indefinite Hermitian Gaussian quadratic form has already been studied by Al-Naffouri *et al.* [32]. Since Eq. (27) is a sum of independent

quadratic forms, its CDF can be derived as a straightforward extension of the results presented in [32]. The CDF of z_g is obtained as

$$F(z_g|x=x_\ell) = \begin{cases} \sum_{j=1}^{K} \frac{(-1)^{K-j} z_g^{j-1}}{j!(K-j)!|\lambda_1|^K} \exp\left(-\frac{z_g}{\lambda_1}\right) a_j(\lambda_1) & z_g < 0 \\ 1 + \sum_{j=1}^{K} \frac{z_g^{j-1}}{j!(K-j)!|\lambda_2|^K} \exp\left(-\frac{z_g}{\lambda_2}\right) a_j(\lambda_2) & z_g \geq 0, \end{cases} \tag{30}$$

where $\lambda_m = \lambda_m(x_\ell) \equiv \lambda_m(\boldsymbol{W}_\ell)$ for $m = 1, 2$, $a_j(\lambda_1)$ $a_j(\lambda_2)$ are partial fraction expansion coefficients that can be calculated using

$$a_j(\lambda_1) = \lim_{\zeta \to \frac{-1}{\lambda_1}} \frac{d^{K-j}}{d\zeta^{K-j}} \frac{1}{\zeta(1+\zeta\lambda_2)^K},$$
$$a_j(\lambda_2) = \lim_{\zeta \to \frac{-1}{\lambda_2}} \frac{d^{K-j}}{d\zeta^{K-j}} \frac{1}{\zeta(1+\zeta\lambda_1)^K}. \tag{31}$$

After calculating the derivatives at the specified limits, this CDF can be used to determine the probability of error in Eq. (7) when V_g is available.

When $K = 1$, this CDF is belongs to an asymmetric-Laplace random variable [33, ch. 3] with scale parameter $\sqrt{-1/(\lambda_1(x_\ell)\lambda_2(x_\ell))}$ and asymmetry parameter $\sqrt{-\lambda_1(x_\ell)/\lambda_2(x_\ell)}$.

IV. Receiver Implementation

The test statistics z_d in Eq. (14) and z_g in Eq. (25) are both difference of quadratic functions of the measurement $\boldsymbol{y}$. Let the matrix $\boldsymbol{G}(x_\ell)$ denote either $\boldsymbol{G}_d(x_\ell)$ defined in Eq. (10) or $\boldsymbol{G}_g(x_\ell)$ defined in Eq. (23) for $\ell = 0, 1$, and similarly let z denote either z_d or z_g so that a general test statistics be defined as

$$z = \sum_{k=1}^{K} \left(\boldsymbol{y}^H[k]\boldsymbol{G}(x_1)\boldsymbol{y}[k] - \boldsymbol{y}^H[k]\boldsymbol{G}(x_0)\boldsymbol{y}[k]\right)$$
$$= \sum_{k=1}^{K} \|\boldsymbol{B}^H(x_1)\boldsymbol{y}[k]\|^2 - \sum_{k=1}^{K} \|\boldsymbol{B}^H(x_0)\boldsymbol{y}[k]\|^2, \tag{32}$$

where $\boldsymbol{B}(x_\ell)$ satisfies $\boldsymbol{G}(x_\ell) = \boldsymbol{B}(x_\ell)\boldsymbol{B}^H(x_\ell)$, and is referred to as *beamforming matrix*. Since $\boldsymbol{G}(x_\ell)$ is Hermitian, $\boldsymbol{B}(x_\ell)$ is also Hermitian so that $\boldsymbol{B}^H(x_\ell) = \boldsymbol{B}(x_\ell)$, and $\boldsymbol{B}(x_\ell)$ is the square root of $\boldsymbol{G}(x_\ell)$. In case the AmBC system assumes constant ambient signal s, the beamforming matrix, denoted as $\boldsymbol{B}_d(x_\ell)$, is equal to $\boldsymbol{G}_d(x_\ell)$, since $\boldsymbol{G}_d(x_\ell)$ is idempotent,

$$\boldsymbol{B}_d(x_\ell) = \boldsymbol{G}_d^{\frac{1}{2}}(x_\ell) = \boldsymbol{G}_d(x_\ell) = \boldsymbol{I} - \frac{\boldsymbol{g}_\ell \boldsymbol{g}_\ell^H}{\|\boldsymbol{g}_\ell\|^2}. \tag{33}$$

For the Gaussian distributed ambient signal s case, it is given by

$$\boldsymbol{B}_g(x_\ell) = \boldsymbol{G}_g^{\frac{1}{2}}(x_\ell) = \boldsymbol{I} - (1 - \frac{1}{\sqrt{1+\sigma_s^2\|\boldsymbol{g}_\ell\|^2}}) \frac{\boldsymbol{g}_\ell \boldsymbol{g}_\ell^H}{\|\boldsymbol{g}_\ell\|^2}. \tag{34}$$

A receiver that makes a decision using the test statistic in Eq. (32) can be implemented as a square-sum device after beamforming $\boldsymbol{y}$ using the matrix $\boldsymbol{B}(x_\ell)$, as illustrated in Fig. 2a. The received signal is split into two streams to feed two branches. Each of the streams goes through a beamformer to calculate $\boldsymbol{B}(x_0)\boldsymbol{y}$ or $\boldsymbol{B}(x_1)\boldsymbol{y}$, and through a square-sum device to calculate their norm-squares. The receiver makes a decision by comparing the difference of the norm-square with the decision threshold V.

The optimum receiver given in Fig. 2a requires i) the beamforming matrices $\boldsymbol{B}(x_0)$ and $\boldsymbol{B}(x_1)$, and ii) the decision threshold value V. In the remaining part of this section, we first present different methods to estimate the beamforming matrices, and thereafter, we discuss the practical details and implications of the presented receivers.

A. Estimation of the Beamformers

The beamformers $\boldsymbol{B}(x_0)$ and $\boldsymbol{B}(x_1)$ are required for constructing the optimum receivers. The beamforming matrices $\boldsymbol{B}(x_\ell)$ can be calculated by estimating the matrix $\boldsymbol{G}(x_\ell)$. These matrices are functions of the conditional auto-correlation matrix of the measurements when the BD symbol is given, which reads as

$$\boldsymbol{R}_{\boldsymbol{y}|x_\ell} = \boldsymbol{\Sigma}_{\boldsymbol{y}|x_\ell} + \mathrm{E}\{\boldsymbol{y}|x=x_\ell\}\mathrm{E}^H\{\boldsymbol{y}|x=x_\ell\}, \tag{35}$$

where $\boldsymbol{\Sigma}_{\boldsymbol{y}|x_\ell}$ is the conditional covariance matrix. For the unknown ambient signal case, the auto-correlation matrix is obtained as

$$\boldsymbol{R}_{\boldsymbol{y}|x_\ell}^{(d)} = \boldsymbol{I} + |s|^2 \boldsymbol{g}_\ell \boldsymbol{g}_\ell^H,$$

whose eigenvalues are $\{1 + \|s\boldsymbol{g}_\ell\|^2, 1, \cdots, 1\}$, and the eigenvector corresponding to its largest eigenvalue is $\boldsymbol{g}_\ell/\|\boldsymbol{g}_\ell\|$. The beamforming matrix $\boldsymbol{B}_d(x_\ell)$ in Eq. (33) is the projection matrix onto the linear subspace orthogonal to the space spanned by the largest eigenvector. The threshold value V_d is constant and equal to 0 when BD symbols have equal probability. For the Gaussian distributed ambient signal case, on the other hand, we have

$$\boldsymbol{R}_{\boldsymbol{y}|x_\ell}^{(g)} = \boldsymbol{I} + \sigma_s^2 \boldsymbol{g}_\ell \boldsymbol{g}_\ell^H,$$

with eigenvalues $\{1+\sigma_s^2\|\boldsymbol{g}_\ell\|^2, 1, \cdots, 1\}$, and the eigenvector corresponding to its largest eigenvalue is $\boldsymbol{g}_\ell/\|\boldsymbol{g}_\ell\|$. For this case, the beamforming matrix $\boldsymbol{B}_g(x_\ell)$ in Eq. (34) can be calculated from the largest eigenvalue and the corresponding eigenvector. The threshold value V_g is the ratio of the largest eigenvalues of the measurement auto-correlation matrices under two hypotheses. In either case, an estimate of $\boldsymbol{R}_{\boldsymbol{y}|x_\ell}$ in Eq. (35) is required.

The auto-correlation matrix estimation has well-known solutions. Among the alternatives, the easiest is to collect samples when a known symbol is transmitted by the BD for a certain duration, referred to as preamble.[4] In particular, two length-P preambles represented by $x[1] = \cdots = x[P] = x_0$ and $x[P+1] = \cdots = x[2P] = x_1$ can be used for estimating $\boldsymbol{R}_{\boldsymbol{y}|x_0}$ and $\boldsymbol{R}_{\boldsymbol{y}|x_1}$, respectively. Let us define the sample matrix of the measurements acquired when the BD is transmitting x_ℓ as

$$\boldsymbol{Y}_\ell = \left[\boldsymbol{y}[1+\ell P] \vdots \quad \cdots \quad \vdots \boldsymbol{y}[P+\ell P]\right] \tag{36}$$

[4]The preamble refers to the preamble transmitted by the BD. The preamble of the ambient system is not needed for estimating the beamformers.

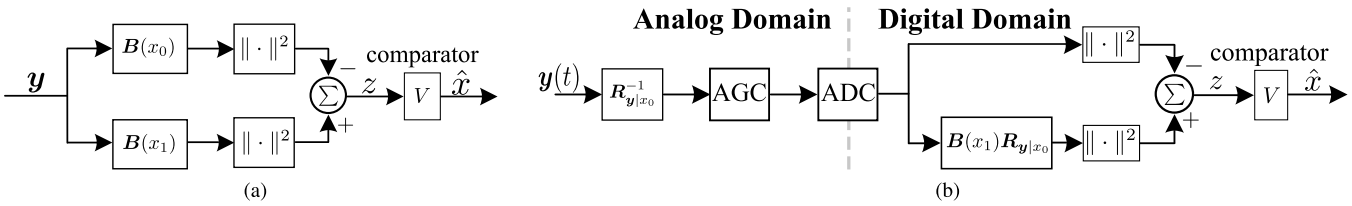

Fig. 2. In (a), implementation of the optimum receiver with two beamformers. In (b), an analog-digital hybrid implementation of the optimum receiver with two beamformers, one in analog domain that suppresses the direct path signal before automatic gain control (AGC) operating before analog-to-digital converter (ADC). The digital beamformers are either $\boldsymbol{B}_d(x_\ell)$ in Eq. (33) or $\boldsymbol{B}_g(x_\ell)$ in Eq. (34) for $\ell = 0, 1$. The analog side beamformer is the inverse of the positive-definite auto-correlation matrix in Eq. (35) for $x = x_0$. The resultant square-sum value of branch x_0 is subtracted from the other branch, and the difference is compared with the decision threshold.

Then, the auto-correlation matrix can be estimated as

$$\hat{\boldsymbol{R}}_{\boldsymbol{y}|x_\ell} = \frac{1}{P}\sum_{p=1}^{P} \boldsymbol{y}[p+\ell P]\boldsymbol{y}^H[p+\ell P] = \frac{1}{P}\boldsymbol{Y}_\ell \boldsymbol{Y}_\ell^H. \quad (37)$$

The conditional measurement auto-correlation matrix estimate $\hat{\boldsymbol{R}}_{\boldsymbol{y}|x_\ell}$ in Eq. (37) converges to a positive definite Hermitian matrix for some $P > N_r$. Let us suppose that P is selected such that $\hat{\boldsymbol{R}}_{\boldsymbol{y}|x_\ell} \approx \boldsymbol{R}_{\boldsymbol{y}|x_\ell}$. Since the optimum receiver only needs the largest eigenvalue and its associated eigenvector, the power method [34, Sec. 8.2.1] is an iterative algorithm to calculate these by

$$\hat{\boldsymbol{u}}^{(\iota+1)} = \frac{\boldsymbol{Y}_\ell \boldsymbol{Y}_\ell^H \hat{\boldsymbol{u}}^{(\iota)}}{\|\boldsymbol{Y}_\ell \boldsymbol{Y}_\ell^H \hat{\boldsymbol{u}}^{(\iota)}\|},$$

for the iteration number $\iota = 0, 1, \cdots$. The calculation is stopped when the eigenvector estimate $\hat{\boldsymbol{u}}^{(\iota)}$ satisfies a convergence criteria for its associated eigenvalue estimate, given by

$$\hat{\lambda}^{(\iota)} = \frac{1}{P}\|\boldsymbol{Y}_\ell^H \hat{\boldsymbol{u}}^{(\iota)}\|^2.$$

This algorithm converges if i) the initial vector $\hat{\boldsymbol{u}}^{(0)}$ has a non-zero and significant component along the largest eigenvector, and ii) the largest eigenvalue is unique, and its separation from the closest eigenvalue is high enough with respect to the machine precision.

For the considered problem this method converges when $|s|^2\|\boldsymbol{g}_\ell\|^2$ or $\sigma_s^2\|\boldsymbol{g}_\ell\|^2$ is high and the eigenvector estimate is initialized appropriately. In practice, the initial estimate of the eigenvector can be set to an estimate of direct path channel $\boldsymbol{\alpha}$, which can be calculated using the measurements acquired when the BD is not operating. Therefore, power iteration is a practically appealing method to find the the largest eigenvalue and associated eigenvector of the measurement auto-correlation matrix to estimate the beamformers.

B. Discussion

The designed receivers are based on the MAP principle, which is equivalent to maximum likelihood (ML) criterion when the BD symbol probabilities are equal. The ML criterion arises naturally in likelihood ratio tests, which is the optimal detector that maximizes the detection probability for a given false alarm rate (significance level) due to Neyman-Pearson Theorem [35, Vol. II, Sec. 3.3]. The equivalent Bayesian approach is derived when prior probabilities of each hypothesis can be assigned, as it is for communication systems. In this case, the MAP criterion, which yields a receiver that minimizes the Bayesian Risk, is the optimal (also referred to as the *strongest*) binary hypothesis test although it does not require a specific false alarm probability to maximize the detection probability [35, Vol. II, Sec. 3.7]. Therefore, the developed receivers are optimal in Bayesian sense and have the lowest probability of error among all possible binary hypothesis tests.

The difference between receivers for Gaussian distributed and deterministic-unknown ambient signal s arises due to the coefficients c_ℓ in Eq. (23). For deterministic-unknown s case $c_\ell = 1$. When the total received SNR of the ambient signal is high, say more than 20 dB, we have $\sigma_s^2\|\boldsymbol{g}_\ell\|^2 > 100$, which implies $c_\ell \approx 1$. In this case, the test statistic z_g in Eq. (25) approximates to z_d in Eq. (14). Furthermore, for Gaussian case the decision threshold in Eq. (25) can be written as

$$V_g = \ln\left(\frac{c_1}{c_0}\frac{\|\boldsymbol{g}_0\|^2}{\|\boldsymbol{g}_1\|^2}\right).$$

For all practical AmBC deployments, the channel gains $\boldsymbol{\alpha}$ and $\boldsymbol{\beta}$ in Eq. (4) has a significant gain difference as discussed earlier. This implies that $\|\boldsymbol{g}_0\|^2/\|\boldsymbol{g}_1\|^2 \approx 1$, and $V_g \approx 0$. Therefore, when total received SNR of the ambient signal is high and the channel gain difference between the direct path and backscatter path is significant, the receivers for deterministic-unknown s and Gaussian distributed s are equivalent. In the remaining part of the discussions, we analyze the supported ambient systems and signals, highlight the physical parameters defining the receiver performance, and investigate possible practical implementation issues. Before we delve into these discussions, let us summarize the advantageous features of the optimum receiver shown in Fig. 2a:

i.) The receiver does not require an explicit ambient signal estimate, but implicitly handles its impact through the beamformers. Furthermore, its operation does not depend on the ambient signal type as long as the ambient system uses a modulation scheme with a symmetrical signal constellation around zero of the complex plane.

ii.) The receiver is a non-coherent receiver since it does not require BD symbol phase. It does not require explicit knowledge of channels $\boldsymbol{\alpha}$ and $\boldsymbol{\beta}$, but only composite channel $\boldsymbol{g}_\ell$ defined in Eq. (4). This channel is estimated for different BD symbols as described in Sec. IV-A.

iii.) The receiver does not assume a specific value for the transmitted BD symbol, and a BD symbol value is solely defined by the preamble sequence. The BD can use any binary tag symbols during one frame transmission without explicitly informing the receiver; it chooses the symbol values during the preamble transmission, and then uses the same values during the frame transmission.

1) Supported Ambient Systems and Signals: The auto-correlation matrix estimate in Eq. (37) using the measurement matrix $\boldsymbol{Y}_\ell$ in Eq. (36) can be written as

$$\hat{\boldsymbol{R}}_{\boldsymbol{y}|x_\ell} = \boldsymbol{g}_\ell \boldsymbol{g}_\ell^H \frac{1}{P} \sum_{p=1}^{P} |s[p+\ell P]|^2 + \boldsymbol{I}, \tag{38}$$

which is valid when P is large, the measurement noise process $\boldsymbol{n}$ is ergodic in wide-sense,[5] it is independent of the ambient signal s, and it has a zero mean. These are all implied by the definition of the measurement noise and selection of the preamble length. This expression also requires the channel gains $\boldsymbol{g}_\ell$ to be constant, which is valid for a block-fading channel with coherence time exceeding the longest frame duration. The square sum of the time samples of s should be finite to guarantee convergence of the sum, which implies that the ambient signal should have a finite power. This requirement is not restrictive for a practical ambient transmitters, since all ambient systems must possess this property. Therefore, for all practical ambient sources, the auto-correlation estimate in Eq. (38) is valid.

In order to investigate what type of ambient signals are supported, let us assume that s is a wide-sense ergodic random process with mean μ_s and variance σ_s^2. Then, the sum in Eq. (38) converges to

$$\frac{1}{P} \sum_{p=1}^{P} |s[p+\ell P]|^2 \to \sigma_s^2 + |\mu_s|^2.$$

The mean $\mu_s = 0$ for all modulation types with signal constellation points symmetrical around the zero of the complex plane.[6] The variance σ_s^2 is defined by the transmitted binary data sequence, modulation type and the spectral properties of the transmitter filter, and for a given transmitter filter and equally probable symbols, the variance can be calculated from the power spectral density of the modulation [27, Sec. 3.4]. For equally probable frequency shift keying and phase shift keying modulations, the variance σ_s^2 is equal to the symbol power, and all symbols have equal amplitude $|s|$. For amplitude shift keying, the variance is equal to the average signal power. The more complex modulations, such as orthogonal frequency division multiplexing, have more involved variance expressions, and their signals can be treated as Gaussian s. Therefore, all ambient signals from symmetrical constellations are supported by the AmBC receiver for deterministic-unknown s, and ambient signals of more complex modulations are supported by the receiver for Gaussian s. Since these two receivers are equivalent when SNR is high, the receiver for deterministic-unknown s supports all types of ambient signals with zero mean.

The derivations in Sec. III assume that the ambient signal s always present. When this assumption fails, the receiver must identify first the presence of s, and then try to decode the BD symbol. This problem has well-known solutions in cognitive radio literature, e.g., the solutions provided by Zhang *et al.* [36]. Since ambient systems that transmit information in a sporadic basis require a more careful AmBC system design, we have not considered such systems in our analysis.

2) Receiver Performance: The existence of BD in the propagation environment inevitably alters the channel between Tx and Rx (direct path channel). This is known as *structural mode* of the BD, and is defined as scattering of the incident signal, which is independent of the BD operation [37]. Its mere impact is to add an additional multipath component to the channel $\boldsymbol{\alpha}$, but does not affect the channel $\boldsymbol{\beta}$. This also implies that the structural mode is not expected to alter the operation of the receiver since the beamformer estimates already contain its impact. The channel models used in this work are general and covers the impact of structural mode, and therefore, the designed receivers do not require any special treatment for this mode.

The channel realizations affect the received signal $\boldsymbol{y}$ in Eq. (4) by changing the vector $\boldsymbol{g}$ so that they should be taken into account when deriving the likelihood functions. However, since the channels assume a single realization during a frame transmission, the conditional density of $\boldsymbol{y}$ for a given BD symbol x can be equivalently written conditioning on $\boldsymbol{g}$, i.e., $f(\boldsymbol{y}|x = x_0) \equiv f(\boldsymbol{y}|\boldsymbol{g} = \boldsymbol{g}_0)$, and $f(\boldsymbol{y}|x = x_1) \equiv f(\boldsymbol{y}|\boldsymbol{g} = \boldsymbol{g}_1)$. This also implies that once the beamformers are estimated, the unknown phase of the backscatter channels are constant throughout the frame transmission. Thus, the derived likelihoods do not depend on the phase, and the receiver does not require phase-coherent operation.

The performance of the receiver depends on the estimation quality of the beamformers. In order to investigate the impact of beamformer estimation error, let us assume that the power iteration has converged to a vector

$$\hat{\boldsymbol{g}}_\ell = \frac{\boldsymbol{g}_\ell + \boldsymbol{e}_\ell}{\|\boldsymbol{g}_\ell + \boldsymbol{e}_\ell\|},$$

such that $\boldsymbol{e}_\ell^H \boldsymbol{g}_\ell = 0$. When $x = x_1$, the noise term independent test statistic in Eq. (14) changes approximately by

$$z_\Delta \approx |s|^2 \left(\frac{\boldsymbol{g}_1^H \boldsymbol{e}_0 \boldsymbol{g}_1^H \boldsymbol{g}_0}{\|\boldsymbol{g}_0 + \boldsymbol{e}_0\|^2} + \frac{\boldsymbol{g}_1^H \boldsymbol{g}_0 \boldsymbol{e}_0^H \boldsymbol{g}_1}{\|\boldsymbol{g}_0 + \boldsymbol{e}_0\|^2} + \frac{|\boldsymbol{g}_1^H \boldsymbol{e}_0|^2}{\|\boldsymbol{g}_0 + \boldsymbol{e}_0\|^2} \right).$$

The common denominator is $\|\boldsymbol{g}_0 + \boldsymbol{e}_0\|^2 = \|\boldsymbol{g}_0\|^2 + \|\boldsymbol{e}_0\|^2$. Thus, the impact of beamformer estimation error should be quantified by both

$$\begin{aligned} b_{e,m} &\triangleq \|\boldsymbol{e}_0\| + \|\boldsymbol{e}_1\|, \text{ and} \\ b_{e,a} &\triangleq \frac{|\boldsymbol{e}_0^H \boldsymbol{g}_1|}{\|\boldsymbol{e}_0\| \|\boldsymbol{g}_1\|} + \frac{|\boldsymbol{e}_1^H \boldsymbol{g}_0|}{\|\boldsymbol{e}_1\| \|\boldsymbol{g}_0\|}. \end{aligned} \tag{39}$$

[5] A random process is ergodic in wide-sense when it is both mean and covariance ergodic.

[6] On-off keying has a non-zero mean. However, since in zero state no energy is transmitted, ambient systems using on-off keying modulation are not considered.

In the next section, we investigate the impact of these on the BER performance.

In general, the benefit of using BPSK modulation compared with OOK is a lower BER for a given SNR value. This can be investigated by observing the eigenvalues in Eq. (28) for Gaussian distributed ambient signal when its SNR is high. For this case, the eigenvalues simplify to

$$\lambda_1(x_0) \approx -\sigma_s^2\|\boldsymbol{g}_0\|^2\kappa^2, \quad \lambda_2(x_0) \approx 1,$$
$$\lambda_1(x_1) \approx -1, \quad \lambda_2(x_1) \approx \sigma_s^2\|\boldsymbol{g}_1\|^2\kappa^2,$$

and the decision threshold is $V_g \approx 0$. Substituting these into Eq. (30) for $K = 1$, and then into Eq. (7) for $z_g = V_g = 0$, the probability of error can be approximated to

$$P_e \approx \frac{1}{2}\left(\frac{1}{1+\sigma_s^2\|\boldsymbol{g}_0\|^2\kappa^2} + \frac{1}{1+\sigma_s^2\|\boldsymbol{g}_1\|^2\kappa^2}\right)$$
$$\approx \frac{1}{2\sigma_s^2\kappa^2}\left(\frac{1}{\|\boldsymbol{g}_0\|^2} + \frac{1}{\|\boldsymbol{g}_1\|^2}\right).$$

Thus, the BER decreases in such a way that the higher κ^2 and $\|\boldsymbol{g}_1\|^2 - \|\boldsymbol{g}_0\|^2$ are, the better the performance is. For BPSK modulation, $\kappa = 1$ when the normalized channels are orthogonal, which also yields $\|\boldsymbol{g}_1\|^2 - \|\boldsymbol{g}_0\|^2 = 2\|\boldsymbol{\beta}\|^2$. However, for OOK modulation we have $\kappa \leq 1/\sqrt{2}$, and $\kappa = 1/\sqrt{2}$ implies $\|\boldsymbol{g}_1\|^2 - \|\boldsymbol{g}_0\|^2 = \|\boldsymbol{\beta}\|^2$. Therefore, for a fixed BER, BPSK requires up to $10\log_{10}(4) \approx 6.02$ dB less SNR.

The received BD signal strength has been studied by Griffin and Durgin [38], and several key parameters affecting the signal strength are identified. The Tx and Rx antenna gains, propagation related losses, the BD antenna gain, and polarization mismatch of the links between Tx and BD, and Rx and BD affect the signal strength. In addition to these, the practical losses due to BD modulator circuit implementation may degrade the BD signal strength. The modulator losses may arise from the mismatch of the antenna impedance, the transmission line characteristic impedance and/or the impedance of the dissipating load, and the non-zero impedance of the switches when they are in 'on' state. In this paper, we make the following simplifying assumptions: 1.) Tx, Rx and BD have ideal isotropic antennas with unity gain; 2.) the links between Tx and BD, and BD and Rx polarization mismatches are ignored by assuming perfect polarization matching; and 3.) the implementation is close to ideal. Since the considered system is the same as bistatic and dislocated backscatter systems [38], under these assumptions, the link budget of the backscatter signal is mainly defined by the propagation losses. The effects of other parameters can be added to the logarithmic propagation losses, for instance, the impact of transmission power, antenna gains etc. If the antennas are directive, their impact can be included by adding/subtracting directive antenna gains for a given BD location. If there is a polarization mismatch, the amount of mismatches can be taken into account by subtracting a positive number since it is a real non-negative constant smaller than 1 in linear scale.

The propagation losses associated with the backscattered signal of an AmBC system operating at 500 MHz is shown in Fig. 3.a, where the path-loss exponents all set to ideal value of 2. Event for this ideal scenario, although the ambient signal experiences only 46.83 dB propagation loss, the BD losses are between 80 and 110 dB. These values imply that the backscatter signal is very weak compared to the strength of the ambient signal, and successful BD operation is possible when it is placed close to either Tx or Rx. Let us consider the well-known large-scale propagation loss model $\mathcal{L}_\eta(d) = \mathcal{L}_0 + 10\eta\log(d)$, where η is the path-loss exponent, $\mathcal{L}_0$ is the loss measured at a reference distance, and d is the link-length scaled with the reference distance. For this model, the direct link experiences a loss of $\mathcal{L}_0 + 10\eta_{tr}\log(d_0)$ dB, while the backscatter path experience $2\mathcal{L}_0 + 10\eta_{tb}\log(d_2) + 10\eta_{br}\log(d_1)$ dB where η_{tr}, η_{tb} and η_{br} are path-loss exponents of the links between Tx and Rx, Tx and BD, and BD and Rx respectively. However, Fig. 3.a implies that η_{tr}, η_{td} and η_{dr} cannot assume arbitrary values. On the contrary, it implies that, when BD is close to Tx, $\eta_{tb} \approx 2$ and $\eta_{br} \approx \eta_{tr}$; and when BD is close to Rx, $\eta_{br} \approx 2$ and $\eta_{tb} \approx \eta_{tr}$. Consequently, the path loss exponent η_{tr} value merely alters the ambient signal power, and scales the SNR of the ambient signal. Therefore, the results presented in Sec. V are valid under different path loss exponents, and its impact on the ambient signal SNR plots in logarithmic scale is just to shift the curves to either left (when $\eta_{tr} < 2$) or right (when $\eta_{tr} > 2$).

The performance of the receiver has a strong dependence on the parameter κ. By definition, it is the absolute value of sine of the rotation angle between $\boldsymbol{g}_0$ and $\boldsymbol{g}_1$, which we refer to as *angular variation*, and takes a real value between 0 and 1. It is 0 when the vectors are parallel, and 1 when they are orthogonal. Correspondingly, κ attains its maximum when the channel gains $\boldsymbol{\beta}$ and $\boldsymbol{\alpha}$ are perpendicular to each other, and its minimum when they are parallel. The two dimensional variation in κ is shown in Fig. 3b. The depicted result implies that the angular variation is the largest when the BD is close to Rx or Tx. Therefore, the derived optimum receiver has the best performance when the BD has a suitable location, and it may perform at its best when BD is within ± 10 wavelength distance from the Rx's location or close the Tx (approximately ± 5 wavelengths).

The channel gains $\boldsymbol{\alpha}$ and $\boldsymbol{\beta}$ defined in Sec. II-C do not discriminate between different fading processes as long as their individual components experience a single realization of the channel gain. This assumption is valid when the environment, the BD, the transmitter and the receiver are all quasi-stationary for the duration of a single BD frame transmission. The small-scale fading changes the observed SNR of both ambient and backscatter signal, and might yield poor receiver performance. The impact of fading losses defined in Eq. (1) on BER performance of Gaussian modulated ambient signal s for the simulated scenario described in Sec. V is shown in Fig. 3. As can be observed, as long as the fading gain ρ_β is larger than 0.6, the receiver performs well. Therefore, the mere impact of small scale fading losses is to shift BER performance curves slightly toward lower SNR values, which can be compensated by increasing number of samples acquired for each backscattering symbol K, and are not considered in Sec. V. Therefore, the derived receivers can handle small-scale

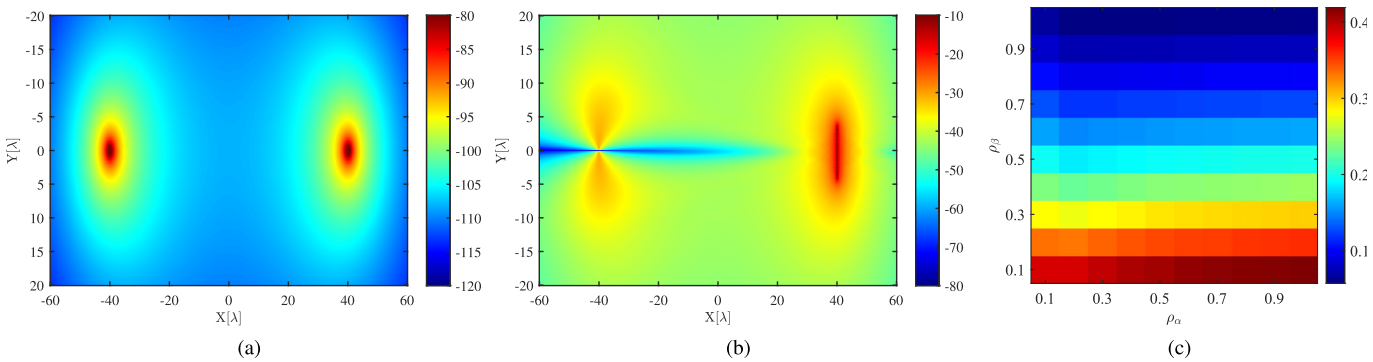

Fig. 3. In (a), the variation in link losses in dB experienced by the backscatter signal at the reference antenna with the backscatter device location when the ambient transmitter is placed $(-40, 0)$ and the reference receive antenna is at $(40, 0)$ and the wavelength λ is 0.6 m. In (b), the variation in $20\log_{10}(\kappa)$ in Eq. (16) with backscatter device location for the same ambient system as in (a), and the number of receiver antennas is $N_r = 16$, backscatter device uses BPSK modulation, and only the free-space path loss is considered when calculating $\boldsymbol{g}_\ell$ defined in Eq. (4). In (c), the variation in bit error rate with fading parameters ρ_α and $\rho_\alpha\beta$ in Eq. (1) for Gaussian ambient signal and BPSK modulated backscattering symbol when SNR $\gamma = 24$ db and oversampling $K = 4$.

fading affects without a need for a special treatment in the receiver architecture.

The projected BD ranges are larger than the reported ranges for different AmBC implementations. For an AmBC system using TV signal as ambient source [2], the transmission distance between a passive BD and Rx is up to 1 meter (1.5 wavelength) when the TV tower (Tx) is more than 4 kilometers away from BD and Rx. In [39], the BD achieves successful communication when the distance between BD and Rx is 50 meters and the distance between Tx and BD is fixed to be 1 meter (4 wavelengths) for the 802.11b ambient signal. The communication range for long-range (LoRa) ambient signal can reach up to 1.1 kilometers between BD and Rx when BD is placed 0.2 meter (less than a wavelength) apart from Tx [40]. The projected ranges can be drastically improved by using time-diversity by increasing the oversampling rate K or using coding. Therefore, the proposed receiver is expected to improve the AmBC system range significantly.

3) Receiver Implementation: The beamformer products in the optimum receiver shown in Fig. 2a at first glance can be implemented as a matrix vector product processors. However, since the beamformers are difference between identity matrix and a rank-one matrix, it requires only one inner product and a vector difference processor. Thus, their hardware implementation requirements are not higher than standard multiantenna receivers. However, the beamformer estimator requires N_r digital streams, which implies that the receiver can be implemented using N_r number of RF front-ends each followed by an analog-to-digital converter (ADC).

The receiver given in Fig. 2a is an example implementation in the digital domain. In practice, the dynamic range of the ADC determines the quality of the numerical representation of the measurement $\boldsymbol{y}$. In this regard, since the direct path channel gains are much stronger than the backscatter path channel gains, the significant bits of the digital value of $\boldsymbol{y}$ are representing the direct path signal, while the backscatter signal is limited toward the least significant bits. One solution to overcome the dynamic range problem is to eliminate the direct path in the analog domain before ADC of the receiver as proposed in [7]. However, this approach requires significant modifications to the receiver since the direct path should be estimated. An alternative solution is to implement one of the beamformers in the analog domain and the other in the digital domain as shown in Fig. 2b. Although this implementation provides practical gains, it requires additional implementation details such as resetting the analog beamformer gains when a frame reception is over. Nonetheless, the receiver shown in Fig. 2b can handle numerical problems that might occur in fully digital implementation. The equivalence of the receiver implementations in Fig. 2a and in Fig. 2b are shown in the next section.

V. Simulation Results

In this section, the optimum receivers are numerically evaluated with respect to their BER performance. We first evaluate the impact of the number of receiver antennas N_r, the preamble length P, and beamformer estimation error and ambient signal type on the BER. Then, the identified set of parameters are used for investigating the achievable BER performance for different types of BD modulations. In this section, we refer to the optimum receiver for Gaussian distributed ambient signal in Eq. (24) as *Gaussian receiver*, and the optimum receiver for deterministic-unknown s in Eq. (13) as *deterministic receiver*.

The numerical evaluation is based on the following assumptions. The system experiences a fading process which can be presumed constant during a frame transmission, and the channel gains $\boldsymbol{\alpha}$ and $\boldsymbol{\beta}$ can be calculated using the free-space path-loss model in Eq. (1) for a receiver with N_r-antennas linear array with half wavelength $\lambda/2$ separation. The deployment scenario is fixed for comparative fairness. The distance between the Tx antenna and the reference Rx antenna is $d_0 = 80\lambda$, and placed in the reference frame shown in Fig. 1a. The BD is placed at $[(40 - 4/\sqrt{2})\lambda, (4/\sqrt{2})\lambda]$ so that $d_1 = 4\lambda$, which corresponds to 33.7 dB gain difference between the channels $\boldsymbol{\alpha}$ and $\boldsymbol{\beta}$. The ambient transmitter emits a random symbol with amplitude $\|s\boldsymbol{\alpha}\|$ so that the average SNR is as defined in Eq. (2). The QPSK and 64-ary QAM symbol bits are drawn from uniform distribution,

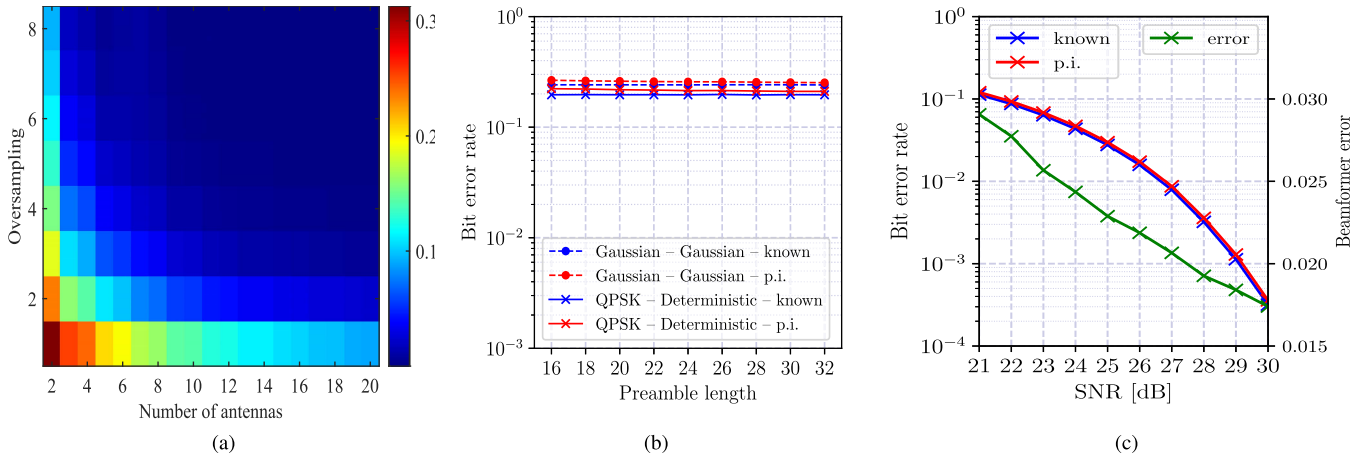

(a) (b) (c)

Fig. 4. Numerical evaluation of the optimum receiver parameters for a backscatter device using BPSK modulation. In (a), variation in Bit Error Rate (BER) of the receiver for Gaussian (in Eq. (24)) ambient signal s with number of antennas N_r and number of samples acquired for each symbol $K$for the mean ambient signal SNR $\gamma = 24$ dB when the beamformers are perfectly known. In (b), variation in the BER of the receivers with preamble length P when the maximum eigenvalue and corresponding eigenvectors of the measurement auto-correlation are perfectly known (known) and when they are estimated using power iteration (p.i.) for $N_r = 4$ and $\gamma = 24$ dB. In (c), variation in the BER and total beamformer estimation error in Eq. (39) with SNR for QPSK modulated ambient signal, $N_r = 4$, oversampling rate $K = 4$ and $P = 32$. The left axis shows the BER of the receivers implemented using perfectly known beamformers and power iteration estimated beamformers. The right axis shows the total beamformer error.

and Gaussian symbols are drawn from standard complex Gaussian distribution. The BD transmits a frame of 1000 symbols drawn from discrete discrete alphabet with equal probabilities, and 1000 realizations are used for calculating the average BER.

In Fig. 4, the impact of different system parameters on the BER performance of the optimum receiver for a BD using BPSK modulation are shown. The impact of number of receiver antennas N_r and oversampling rate K on the BER of the Gaussian ambient signal is studied in Fig. 4a. The acceptable BER is achieved when $N_r \geq 4$ and $K \geq 4$, and for the following evaluations we fix $N_r = 4$ and $K = 4$. In Fig. 4b, the impact of preamble length P on the BER performance is shown when $K = 1$. The receiver is implemented using perfectly known beamformers or *power iteration* (p.i.) (maximum 10 iterations for 10^{-16} tolerance level) estimated beamformers. When s is Gaussian distributed signal, the two Gaussian receiver implementations have negligible performance difference in the considered parameter ranges. For QPSK modulated ambient signal, the implementations have a small BER performance difference, but the difference decreases with increasing P. Thus, the preamble length $P = 32$ provides enough samples for power iteration to estimate the beamformers. The impact of the total beamformer estimation error $b_{e,m} + b_{e,a}$ defined in Eq. (39) is shown in Fig. 4c, where both BER and beamformer error is depicted for QPSK modulated ambient signal. In this evaluation, we omit Gaussian distributed ambient signal case since the estimation error is the same as it is for QPSK modulated ambient signal, and for $P = 32$, BER difference between perfectly known beamformers and power iteration estimated beamformers is negligible. As can be observed, the total beamformer estimation error degrades the observed SNR by small amount, and gets smaller when the system SNR increases. Once the SNR exceeds 25 dB, the estimation error gets smaller than 0.03, and the SNR penalty can be safely ignored.

The BER performance of an N_r-antenna optimal receiver for different ambient signals and binary modulated BD signals are shown in Fig. 5. The impact of ambient signal modulation on the BER performance is shown in Fig. 5a, where three different signals are studied. When s is Gaussian distributed, both Gaussian and deterministic receivers have the same performance. This is because for Gaussian distributed s, its amplitude has a high variability, whereas for QPSK it is constant. An intermediate case is when s is 64-ary QAM modulated. This modulation introduces some variability on the amplitude of s, but its entropy is smaller than Gaussian distributed s case. Correspondingly, M-ary QAM is expected to have a performance close to QPSK modulated s case when M is low, and approaches to Gaussian s performance as M increases. Therefore, the deterministic receiver in Eq. (13) can handle different types of ambient signals, but it has different performance. In Fig. 5b, the BER performance variation of different receivers with average SNR γ and ambient signal type is shown. When ambient signal s is Gaussian distributed, the derived CDF function of the test statistics z_g in Eq. (30) has the same result as the BER curve obtained by simulations. Similarly, for QPSK modulated s, the BER result of the CDF in Eq. (20) is very close to the BER curve of the simulations. The same conclusions are valid also for BPSK modulated tag signals shown in Fig. 5c. Therefore, the performance analysis in Sections III-A2 and III-B2 are valid, and the CDF in Eq. (30) for OOK modulated tag can be used for receivers in the earlier literature to evaluate their expected performance. In particular, since the receiver for Gaussian distributed ambient signal for OOK modulation is the same as the one studied in [8], the benefits of using BPSK modulated BD signal and

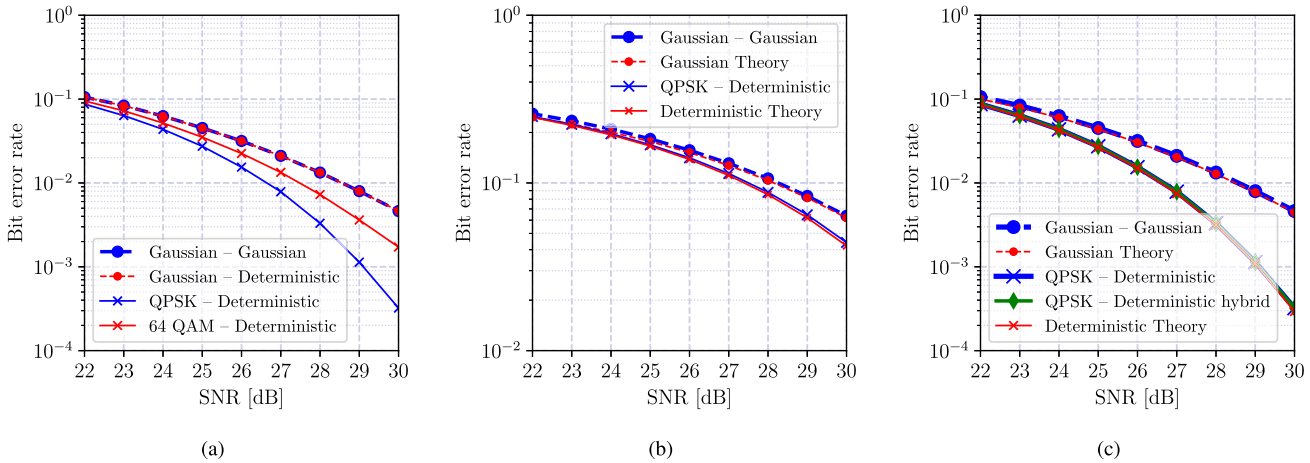

Fig. 5. Variation in Bit Error Rate (BER) of the receivers for Gaussian (in Eq. (24)) and for deterministic-unknown (in Eq. (13)) ambient signal s as a function of mean ambient signal SNR γ when the beamformers are perfectly known for a number of receiver antennas $N_r = 4$ and oversampling rate $K = 4$. The legend uses *ambient signal type – receiver type* notation for numerical results, and theoretical BER curves are indicated with their names. The *Gaussian Theory* curves are calculated using the CDF in Eq. (30), *Deterministic Theory* curves are calculated using the CDF in Eq. (20). In (a), the ambient signal is Gaussian distributed, 64-QAM and QPSK modulated when BD uses BPSK modulation. In (b), the BD uses OOK modulation, and in (c), BPSK modulation.

the generality of the proposed receiver are implied by the results shown in Figures 5b and 5c. The BER performance of the analog-digital hybrid receiver in Fig. 2b is also shown in Fig. 5c (see the curve QPSK – Deterministic hybrid). It has the same performance as digital only implementation, and can be used as a practically advantageous implementation of the optimum receiver.

VI. Conclusion

In this paper, the optimum multiantenna ambient backscatter communication (AmBC) receiver for any binary modulated tag signal is presented. Starting from the maximum-a-posterior probability criterion, different optimum receivers are derived for deterministic-unknown and Gaussian distributed ambient signals separately. The cumulative distribution functions of the test statistics for both of the receivers are derived. The conditions on equivalence of these receivers are identified, and it is concluded that the receiver for deterministic-unknown ambient signal can be used as is with Gaussian distributed ambient signals. The resultant receiver is composed of two beamformers, and practical solutions to several implementation issues are provided. It is discussed that the developed optimum receiver generalizes the multiantenna AmBC receivers presented earlier in the literature while having practically appealing advantages. In particular, the receiver does not assume a particular tag symbol value, and the tag is free to switch between different modulations on the fly. Although its operation does not require explicit tag signal phase estimate, its performance is close to the performance of the phase-coherent receivers of phase modulated tag signals. The receiver does not necessitate explicit ambient signal estimate, but the impact of ambient signal is mitigated implicitly by the beamformers. Therefore, the work in this paper enables a high-performance and practical multiantenna receivers that can support several AmBC applications.

Appendix A
Proof of Proposition I

The range space of the matrix $\boldsymbol{M}_d$ in Eq. (15) is spanned by vectors $\boldsymbol{g}_0$ and $\boldsymbol{g}_1$ so that it is a rank-2 matrix with only two non-zero eigenvalues. In order to find these non-zero eigenvalues, we invoke a well-known theorem in matrix analysis, which states that the non-zero eigenvalues of the product of two normal matrices $\boldsymbol{A}$ and $\boldsymbol{B}$, say $\boldsymbol{AB}$, has the same eigenvalues as $\boldsymbol{BA}$ (see, e.g., [41, Theorem 1.3.22]). To this end, we rewrite

$$\boldsymbol{M}_d = \frac{\boldsymbol{g}_0\boldsymbol{g}_0^H}{\|\boldsymbol{g}_0\|^2} - \frac{\boldsymbol{g}_1\boldsymbol{g}_1^H}{\|\boldsymbol{g}_1\|^2} = \begin{bmatrix} \dfrac{\boldsymbol{g}_0}{\|\boldsymbol{g}_0\|^2} & -\dfrac{\boldsymbol{g}_1}{\|\boldsymbol{g}_1\|^2} \end{bmatrix} \begin{bmatrix} \boldsymbol{g}_0^H \\ \boldsymbol{g}_1^H \end{bmatrix},$$

which has the same non-zero eigenvalues as

$$\begin{bmatrix} \boldsymbol{g}_0^H \\ \boldsymbol{g}_1^H \end{bmatrix} \begin{bmatrix} \dfrac{\boldsymbol{g}_0}{\|\boldsymbol{g}_0\|^2} & -\dfrac{\boldsymbol{g}_1}{\|\boldsymbol{g}_1\|^2} \end{bmatrix} = \begin{bmatrix} 1 & -\dfrac{\boldsymbol{g}_0^H\boldsymbol{g}_1}{\|\boldsymbol{g}_1\|^2} \\ \dfrac{\boldsymbol{g}_1^H\boldsymbol{g}_0}{\|\boldsymbol{g}_0\|^2} & -1 \end{bmatrix}.$$

Therefore, the non-zero eigenvalues of $\boldsymbol{M}_d$ are $\pm\kappa$, defined in Eq. (16), and the corresponding normalized eigenvectors are as given in Eq. (17).

Appendix B
Proof of Proposition II

The non-zero eigenvalues of the matrix $\boldsymbol{\Sigma}_{\boldsymbol{y}|x}^{1/2}\boldsymbol{M}_g\boldsymbol{\Sigma}_{\boldsymbol{y}|x}^{1/2}$ can be obtained by repeatedly applying the Theorem [41, Theorem 1.3.22] as in Appendix A. Applying the theorem for the first time yields that the matrix $\boldsymbol{\Sigma}_{\boldsymbol{y}|x}^{1/2}\boldsymbol{M}_g\boldsymbol{\Sigma}_{\boldsymbol{y}|x}^{1/2}$ has the same non-zero eigenvalues as $\boldsymbol{M}_g\boldsymbol{\Sigma}_{\boldsymbol{y}|x}$. Since the eigenvalues of this matrix for $x = x_1$ can be found exactly the same way as it is for $x = x_0$ case, here we just show the $x = x_0$ case. Now, we have

$$\boldsymbol{M}_g\boldsymbol{\Sigma}_{\boldsymbol{y}|x_0} = \left[\left(c_0\sigma_s^2 + \frac{c_0}{\|\boldsymbol{g}_0\|^2}\right)\boldsymbol{g}_0 - \frac{c_1\sigma_s^2\boldsymbol{g}_1^H\boldsymbol{g}_0}{\|\boldsymbol{g}_1\|^2}\boldsymbol{g}_1 \; -\frac{c_1}{\|\boldsymbol{g}_1\|^2}\boldsymbol{g}_1\right]\begin{bmatrix}\boldsymbol{g}_0^H \\ \boldsymbol{g}_1^H\end{bmatrix}.$$

Applying the theorem one more time yields

$$\begin{bmatrix} \boldsymbol{g}_0^H \\ \boldsymbol{g}_1^H \end{bmatrix} \left[\left(c_0\sigma_s^2 + \frac{c_0}{\|\boldsymbol{g}_0\|^2} \right) \boldsymbol{g}_0 - \frac{c_1\sigma_s^2 \boldsymbol{g}_1^H \boldsymbol{g}_0}{\|\boldsymbol{g}_1\|^2} \boldsymbol{g}_1 \quad -\frac{c_1}{\|\boldsymbol{g}_1\|^2}\boldsymbol{g}_1 \right] = \begin{bmatrix} \sigma_s^2 \|\boldsymbol{g}_0\|^2 \kappa_1^2 & -c_1 \dfrac{\boldsymbol{g}_0^H \boldsymbol{g}_1}{\|\boldsymbol{g}_1\|^2} \\ c_1 \dfrac{\boldsymbol{g}_1^H \boldsymbol{g}_0}{\|\boldsymbol{g}_1\|^2} & -c_1 \end{bmatrix},$$

where κ_1 is defined in Eq. (29). The non-zero eigenvalues of the last 2×2 matrix are the roots of its characteristics polynomial, which yields the eigenvalues given in Eq. (28).

REFERENCES

[1] P. Jonsson *et al.*, "Ericsson mobility report," Ericsson, Stockholm, Sweden, Tech. Rep. EAB-19:007381, Nov. 2019.

[2] V. Liu, A. Parks, V. Talla, S. Gollakota, D. Wetherall, and J. R. Smith, "Ambient backscatter: Wireless communication out of thin air," in *Proc. ACM SIGCOMM*, Hong Kong, 2013, pp. 39–50.

[3] G. Yang, Y.-C. Liang, R. Zhang, and Y. Pei, "Modulation in the air: Backscatter communication over ambient OFDM carrier," *IEEE Trans. Commun.*, vol. 66, no. 3, pp. 1219–1233, Mar. 2018.

[4] M. A. ElMossallamy, M. Pan, R. Jäntti, K. G. Seddik, G. Y. Li, and Z. Han, "Noncoherent backscatter communications over ambient OFDM signals," *IEEE Trans. Commun.*, vol. 67, no. 5, pp. 3597–3611, May 2019.

[5] Z. Mat, T. Zeng, G. Wang, and F. Gao, "Signal detection for ambient backscatter system with multiple receiving antennas," in *Proc. IEEE 14th Can. Workshop Inf. Theory (CWIT)*, Jul. 2015, pp. 50–53.

[6] H. Guo, Q. Zhang, S. Xiao, and Y. C. Liang, "Exploiting multiple antennas for cognitive ambient backscatter communication," *IEEE Internet Things J.*, vol. 6, no. 1, pp. 765–775, Feb. 2019.

[7] R. Duan, E. Menta, H. Yigitler, R. Jantti, and Z. Han, "Hybrid beamformer design for high dynamic range ambient backscatter receivers," in *Proc. IEEE Int. Conf. Commun. Workshops (ICC Workshops)*, May 2019, pp. 1–6.

[8] Q. Tao, C. Zhong, X. Chen, H. Lin, and Z. Zhang, "Optimal detection for ambient backscatter communication systems with multiantenna reader under complex Gaussian illuminator," *IEEE Internet Things J.*, vol. 7, no. 12, pp. 11371–11383, Dec. 2020.

[9] T. Kim and W. Lee, "AnyScatter: Eliminating technology dependency in ambient backscatter systems," in *Proc. IEEE Conf. Comput. Commun. (INFOCOM)*, Jul. 2020, pp. 287–296.

[10] G. Yang, Q. Zhang, and Y.-C. Liang, "Cooperative ambient backscatter communications for green Internet-of-Things," *IEEE Internet Things J.*, vol. 5, no. 2, pp. 1116–1130, Apr. 2018.

[11] A. N. Parks, A. Liu, S. Gollakota, and J. R. Smith, "Turbocharging ambient backscatter communication," in *Proc. ACM SIGCOMM*, Chicago, IL, USA, 2014, pp. 619–630.

[12] G. Wang, F. Gao, R. Fan, and C. Tellambura, "Ambient backscatter communication systems: Detection and performance analysis," *IEEE Trans. Commun.*, vol. 64, no. 11, pp. 4836–4846, Nov. 2016.

[13] G. Vougioukas and A. Bletsas, "Switching frequency techniques for universal ambient backscatter networking," *IEEE J. Sel. Areas Commun.*, vol. 37, no. 3, pp. 464–477, Feb. 2019.

[14] C.-H. Kang, W.-S. Lee, Y.-H. You, and H.-K. Song, "Signal detection scheme in ambient backscatter system with multiple antennas," *IEEE Access*, vol. 5, pp. 14543–14547, 2017.

[15] R. Duan, R. Jantti, M. ElMossallamy, Z. Han, and M. Pan, "Multi-antenna receiver for ambient backscatter communication systems," in *Proc. IEEE 19th Int. Workshop Signal Process. Adv. Wireless Commun. (SPAWC)*, Kalamata, Greece, Jun. 2018, pp. 1–5.

[16] Q. Tao, C. Zhong, X. Chen, H. Lin, and Z. Zhang, "Maximum-eigenvalue detector for multiple antenna ambient backscatter communication systems," *IEEE Trans. Veh. Technol.*, vol. 68, no. 12, pp. 12411–12415, May 2019.

[17] D. Tse and P. Viswanath, *Fundamentals of Wireless Communication*. Cambridge, U.K.: Cambridge Univ. Press, 2005.

[18] X. Wang, R. Duan, H. Yigitler, E. Menta, and R. Jantti, "Machine learning-assisted detection for BPSK-modulated ambient backscatter communication systems," in *Proc. IEEE Global Commun. Conf. (GLOBECOM)*, Dec. 2019, pp. 1–6.

[19] X. Wang, H. Yigitler, R. Duan, E. Y. Menta, and R. Jantti, "Coherent multiantenna receiver for BPSK-modulated ambient backscatter tags," *IEEE Internet Things J.*, vol. 9, no. 2, pp. 1197–1211, Jan. 2021.

[20] J. Qian, F. Gao, G. Wang, S. Jin, and H. Zhu, "Noncoherent detections for ambient backscatter system," *IEEE Trans. Wireless Commun.*, vol. 16, no. 3, pp. 1412–1422, Mar. 2017.

[21] R. G. Gallager, *Principles of Digital Communication*. Cambridge, U.K.: Cambridge Univ. Press, 2008.

[22] S. J. Thomas and M. S. Reynolds, "A 96 Mbit/sec, 15.5 pJ/bit 16-QAM modulator for UHF backscatter communication," in *Proc. IEEE Int. Conf. RFID (RFID)*, Apr. 2012, pp. 185–190.

[23] D. Bharadia, K. R. Joshi, M. Kotaru, and S. Katti, "BackFi: High throughput WiFi backscatter," in *Proc. ACM Conf. Special Interest Group Data Commun.*, Aug. 2015, pp. 283–296.

[24] J. M. Wozencraft and I. M. Jacobs, *Principles of Communication Engineering*. New York, NY, USA: Wiley, 1965.

[25] H. W. Sorenson, *Parameter Estimation: Principles and Problems*, vol. 9. New York, NY, USA: M. Dekker, 1980.

[26] C. R. Rao, *Linear Statistical Inference and its Applications*, 2nd ed. Hoboken, NJ, USA: Wiley, 2008.

[27] J. Proakis and M. Salehi, *Digital Communications*, 5th ed. New York, NY, USA: McGraw-Hill, 2008.

[28] S. B. Provost and E. M. Rudiuk, "The exact distribution of indefinite quadratic forms in noncentral normal vectors," *Ann. Inst. Stat. Math.*, vol. 48, no. 2, pp. 381–394, Jun. 1996.

[29] N. Johnson, S. Kotz, and N. Balakrishnan, *Continuous Univariate Distributions*, vol. 2. Hoboken, NJ, USA: Wiley, 1995.

[30] M. Abramowitz and I. A. Stegun, *Handbook of Mathematical Functions: With Formulas, Graphs, and Mathematical Tables*. New York, NY, USA: Dover, 1970.

[31] M. S. Paolella, *Intermediate Probability: A Computational Approach*. Hoboken, NJ, USA: Wiley, 2007.

[32] T. Y. Al-Naffouri, M. Moinuddin, N. Ajeeb, B. Hassibi, and A. L. Moustakas, "On the distribution of indefinite quadratic forms in Gaussian random variables," *IEEE Trans. Commun.*, vol. 64, no. 1, pp. 153–165, Jan. 2016.

[33] S. Kotz, T. Kozubowski, and K. Podgorski, *The Laplace Distribution and Generalizations: A Revisit with Applications to Communications, Economics, Engineering, and Finance* (Progress in Mathematics). Boston, MA, USA: Birkhäuser, 2001.

[34] G. H. Golub and C. F. Van Loan, *Matrix Computations*, 4th ed. Baltimore, MD, USA: Johns Hopkins Univ. Press, 2013.

[35] S. M. Kay, *Fundamentals of Statistical Signal Processing. Detection Theory*. Upper Saddle River, NJ, USA: Prentice-Hall, 1998.

[36] R. Zhang, T. J. Lim, Y.-C. Liang, and Y. Zeng, "Multi-antenna based spectrum sensing for cognitive radios: A GLRT approach," *IEEE Trans. Commun.*, vol. 58, no. 1, pp. 84–88, Jan. 2010.

[37] J. C. Bolomey, S. Capdevila, L. Jofre, and J. Romeu, "Electromagnetic modeling of RFID-modulated scattering mechanism. Application to tag performance evaluation," *Proc. IEEE*, vol. 98, no. 9, pp. 1555–1569, Sep. 2010.

[38] J. D. Griffin and G. D. Durgin, "Complete link budgets for backscatter-radio and RFID systems," *IEEE Antennas Propag. Mag.*, vol. 51, no. 2, pp. 11–25, Apr. 2009.

[39] P. Zhang, D. Bharadia, K. Joshi, and S. Katti, "HitchHike: Practical backscatter using commodity WiFi," in *Proc. 14th ACM Conf. Embedded Netw. Sensor Syst. (CD-ROM)*, New York, NY, USA, Nov. 2016, pp. 259–271.

[40] Y. Peng *et al.*, "PLoRa: A passive long-range data network from ambient Lora transmissions," in *Proc. Conf. ACM Special Interest Group Data Commun.*, Budapest, Hungary, Aug. 2018, pp. 147–160.

[41] R. A. Horn and C. R. Johnson, *Matrix Analysis*, 2nd ed. New York, NY, USA: Cambridge Univ. Press, 2012.

Hüseyin Yiğitler received the B.Sc. and M.Sc. degrees in electrical and electronics engineering from Middle East Technical University, Ankara, Turkey, in 2004 and 2006, respectively, and the Ph.D. degree from the School of Electrical Engineering, Aalto University, in 2018. He is currently a University Teacher at Aalto University, and taking the Chief Technology Officer role at Biyomod, Ankara. His research interests include RF propagation, localization and tracking, signal processing, and design and implementation of embedded (wireless) systems.

Xiyu Wang (Graduate Student Member, IEEE) received the B.Eng. degree in computer science and technology from Northeast Electric Power University, Jilin, China, in 2015, and the M.Eng. degree in computer science and technology from Beijing Jiaotong University, Beijing, China, in 2018. She is currently pursuing the Ph.D. degree with the Department of Communications and Networking, Aalto University, Espoo, Finland. Her research interests include the receiver design and the performance analysis of backscatter-type of communication for the Internet of Things. She is a Grant Recipient awarded by the China Scholarship Council.

Riku Jäntti (Senior Member, IEEE) received the M.Sc. degree (Hons.) in electrical engineering and the D.Sc. degree (Hons.) in automation and systems technology from the Helsinki University of Technology (TKK) in 1997 and 2001, respectively. He is currently a Full Professor of communications engineering and the Head of the Department of Communications and Networking, School of Electrical Engineering, Aalto University, Finland. Prior to joining Aalto (formerly known as TKK) in August 2006, he was a Professor Pro Tem at the Department of Computer Science, University of Vaasa. His research interests include machine type communications, disaggregated radio access networks, backscatter communications, quantum communications, and radio frequency inference. He is a member of the Editorial Board of the IEEE TRANSACTIONS ON COGNITIVE COMMUNICATIONS AND NETWORKING. He has also been a IEEE VTS Distinguished Lecturer (Class 2016).